CSIRO

Exploration and Mining Report 627R

QUANTITATIVE ANALYSIS OF MAGNETIC MINERALOGY OF PYRRHOTITE-BEARING SAMPLES FROM MOUNT ISA (QUEENSLAND), RENISON BELL (TASMANIA), SCUDDLES (W.A.) AND TWO WESTERN AUSTRALIAN NICKEL DEPOSITS

D.A. Clark

REPORT PREPARED FOR G. FALLON, MIM EXPLORATION

June 1999

RESTRICTED CIRCULATION

This report is not to be cited in other documents without the consent of CSIRO Exploration and Mining

Distribution List

Copy no. .... of 7 copies

TABLE OF CONTENTS Page no.

List of Tables Page no.

List of Figures Page no.

Executive summary

A suite of 12 samples of pyrrhotite-bearing massive sulphide ores from Queensland, Tasmania and Western Australia was submitted by G. Fallon of MIM Exploration Ltd for magnetic property measurements and quantitative analysis of magnetic mineralogy, including estimation of monoclinic and hexagonal pyrrhotite contents. The relationships between magnetic properties/magnetic mineralogy and other petrophysical properties, particularly electrical properties, may be useful for in-mine exploration and ore grade estimation.

The collection included seven copper ore samples from Mount Isa, two tin ore samples from Renison Bell, a sample from the Scuddles Cu-Zn VMS deposit and two samples from pentlandite-pyrrhotite nickel orebodies, L2 from the northern Norseman-Wiluna greenstone belt and W1 from the central Norseman-Wiluna belt.

A new method for estimation of monoclinic and hexagonal pyrrhotite contents of sulphide-bearing samples, based on high temperature hysteresis loops has been developed and tested against conventional thermomagnetic methods. The hysteresis method can be shown to be more sensitive and quantitative than other methods and could be routinely applied to determining the magnetic mineralogy of large collections of samples.

The results confirm that mixed monoclinic and hexagonal pyrrhotites are very common in sulphide ores. 5C intermediate pyrrhotite, with composition ~ Fe_9S_{10}, is the most common "hexagonal' pyrrhotite phase in this collection. The Mount Isa copper ores contain mixed pyrrhotites with subequal amounts of monoclinic and 5C hexagonal pyrrhotite, as well as minor amounts of magnetite. Tin ores from Renison also contain mixed pyrrhotites, Scuddles Zn-Cu ore contains magnetite and hexagonal pyrrhotite, without monoclinic pyrrhotite. One magnetic nickel ore from Western Australia contains predominantly 5C hexagonal pyrrhotite, with substantial monoclinic pyrrhotite. The other, weakly magnetic, nickel ore contains traces of magnetite as the only ferrimagnetic phase, with abundant Fe-rich hexagonal pyrrhotite ± troilite.

1. Introduction

A suite of 12 samples of pyrrhotite-bearing massive sulphide ores from Queensland, Tasmania and Western Australia was submitted by G. Fallon of MIM Exploration Ltd for magnetic property measurements and quantitative analysis of magnetic mineralogy, including estimation of monoclinic and hexagonal pyrrhotite contents. The relationships between magnetic properties/magnetic mineralogy and other petrophysical properties, particularly electrical properties, may be useful for in-mine exploration and ore grade estimation.

The collection included seven copper ore samples from Mount Isa, two tin ore samples from Renison Bell, a sample from the Scuddles Cu-Zn VMS deposit and two samples from pentlandite-pyrrhotite nickel orebodies, L2 from the northern Norseman-Wiluna greenstone belt and W1 from the central Norseman-Wiluna belt.

2. Methods

Standard palaeomagnetic specimens, 2.5 cm in diameter and 2.2 cm long were cut from the samples. Bulk magnetic susceptibilities were measured using the CSIRO low frequency (211 Hz) transformer bridge. An operating frequency well below 1 kHz ensures that conductivity effects on measured susceptibilities are negligible (Clark, 1980). For each specimen, the natural remanent magnetisation (NRM) was measured on a Digico fluxgate spinner magnetometer. Corresponding Koenigsberger ratios (Q) were calculated using a nominal geomagnetic field intensity of 0.5 Oe (50,000 nT).

Densities were measured by the standard technique of weighing in air and water and were used to convert from volume to mass susceptibilities/magnetisations, and vice versa.

Discs, 2.5 cm in diameter and 0.4 mm thick, were sliced from the standard specimens for use in a modified Arun Electronics hysteresis loop tracer. Quasi-saturation magnetisations of these subsamples, in fields of up to 4000 Oe (0.4 T), were determined with the hysteresis loop tracer, which was calibrated using accurately measured masses of pure magnetite (saturation magnetisation 480 G = 480 kA/m, equivalent to a specific saturation magnetisation of 92 emu/g = 92 Am²/kg) dispersed within discs of epoxy resin.

After receipt of the samples a new, highly sensitive and accurately calibrated instrument, capable of measuring high and low field magnetisations of small samples over a wide temperature range, was acquired. This Variable Field Translation Balance (VFTB), built by N. Petersen at the University of Munich Department of Pure and Applied Geophysics, was used to produce high-field thermomagnetic (J_s-T) curves and high-field (maximum field ~8000 Oe = 0.8 T) hysteresis loops at room temperature and a range of elevated temperatures.

The method of thermomagnetic analysis due to Lowrie (1990) was also applied to specimens from each of the samples.

3. Bulk Magnetic Properties

Table 1 gives the densities, mass and volume susceptibilities, NRM intensities and Koenigsberger ratios for all specimens cut from the samples and Table 2 lists sample mean densities, mass and volume susceptibilities, and saturation magnetisations.

Susceptibilities range from very low values (~100 μG/Oe $\approx$ 0.0013 SI, i.e. in the high paramagnetic range) to very high values (up to ~0.05 G/Oe $\approx$ 0.63 SI for a Scuddles ore specimen), reflecting mainly the monoclinic pyrrhotite and magnetite contents. Most of the samples have moderate to high susceptibilities (~1000-5000 μG/Oe $\approx$ 0.013-0.063 SI), comparable to the susceptibilities typical of fresh basalts, or two to three times higher.

Densities range from values comparable to those of intermediate igneous rocks (~2.75 g/cm^3) to values close to that of massive pyrrhotite or pyrite, depending on the sulphide content. There is a weak correlation between susceptibility and density (correlation coefficient = +0.3), reflecting the high densities of monoclinic pyrrhotite (4.6 g/cm^3) and magnetite (5.2 g/cm^3).

NRM intensities are generally strong, except for the essentially paramagnetic sample W1. Koenigsberger ratios are high, usually greater than unity, often much greater than 10. This is typical of samples that contain monoclinic pyrrhotite (Clark, 1983).

4. Qualitative Thermomagnetic Analysis

Clark (1983, 1984, 1985) has reviewed the crystallography, mineralogy and intrinsic magnetic properties of the pyrrhotite group. Pyrrhotites have the general formula $Fe_{1-x}S$, with $0 \leq x \leq 0.13$. Thus the compositions range from FeS to ~Fe_7S_8. Near stoichiometric FeS ($x \leq 0.02$) is known as troilite, which is only stable under highly reducing conditions. Troilite is common in meteorites, but relatively rare in terrestrial environments, where it is mainly restricted to serpentinised ultramafic rocks. Pyrrhotite crystal structures are based on the hexagonal NiAs structure shown in Fig.1. Above the α-transition at 140°C, troilite has the 1C NiAs structure, but at ambient temperatures small dispacements of the Fe and S atoms from the ideal positions produce a superstructure that repeats every two NiAs unit cells along the hexagonal c-axis. This low temperature troilite structure is known as "2C".

Due to ordering of vacanies between the Fe layers, all pyrrhotites have superstructures of the (1A, 1C) NiAs structure, depending on composition, temperature and, particularly over the laboratory time scale, thermal history. Common naturally occurring varieties of pyrrhotite include:

- monoclinic pyrrhotite, which is the most iron-deficient of the pyrrhotite group (composition ~Fe_7S_8; ~46.7 at. % Fe) and has a 4C superstructure, with alternating planes of complete and incomplete Fe layers along the c-axis (Fig.2),
- 5C intermediate pyrrhotite, with composition ~Fe_9S_{10}; ~47.4at. % Fe,
- 11C intermediate pyrrhotite, with composition ~$Fe_{10}S_{11}$; ~47.6 at. % Fe,
- 6C intermediate pyrrhotite, with composition ~$Fe_{11}S_{12}$; ~47.8 at. % Fe.

Fig.1. (facing page) (a) Hexagonal unit cell of the NiAs structure on which structures of the pyrrhotite group are based. Closed circles indicate iron atoms, open circles with dots are sulphur atoms. The iron atoms are stacked in identical layers forming hexagonal prisms, each consisting of six trigonal prisms, which are indicated by shading of the triangular faces. The sulphur layers follow the stacking sequence ABABA...

The unit cell has been expanded to show the atomic arrangement clearly. In fact the atoms are in contact, the sulphurs are arranged in the hexagonal close-packed configuration with the iron atoms occupying all the octahedral interstices. This structure is known as 1C and is adopted by troilite above about 215°C (the α-transition) and by the $Fe_{1-x}S$ solid solution at high temperatures.

(b) The central Fe atom of 1(a), illustrating the 6-fold octahedral (antiprismatic co-ordination of S atoms about the Fe atoms in the 1C structure.

(c) The 6-fold prismatic co-ordination of Fe atoms about the S atoms in the 1C structure.

(a)

A

3·4 Å

2·9 Å

C

(b)

(c)

Analysis of pyrrhotite - Report Prepared for MIM Exploration
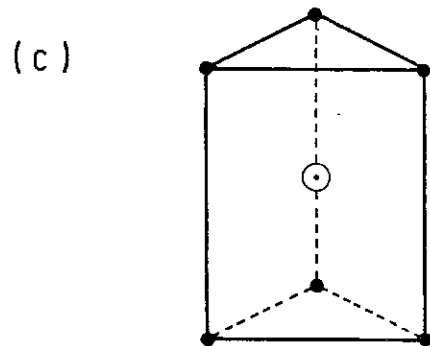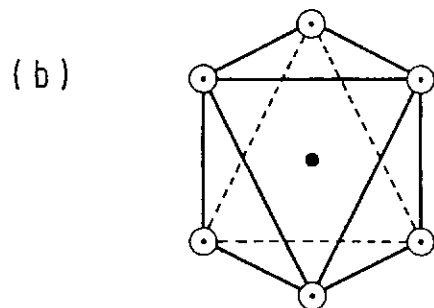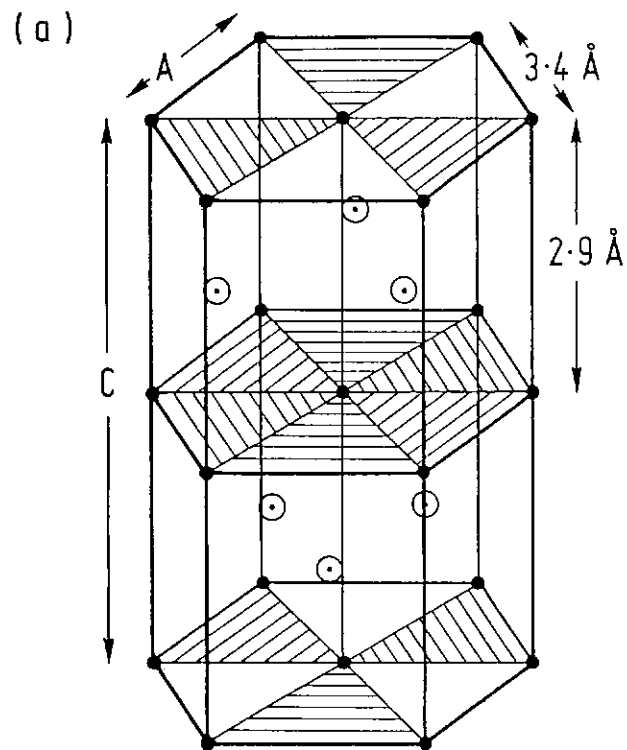
Fig.2. (facing page) The structure of 4C monoclinic pyrrhotite, Fe_7S_8 (Bertaut, 1953).
Alternate iron layers contain vacancies, which are ordered as shown. The orthorhombic 4C
unit cell is shown with the S atoms and the complete Fe layers omitted for clarity. Fe layers are
numbered. There is a slight monoclinic distortion of the orthorhombic unit cell (β = 90.5°),
which has space group F2/d. A smaller monoclinic cell (indicated by dashed lines), which has
symmetry C2/c and lattice parameters a = 2$\sqrt{3}$ A; b = 2A; c = 2C; β = 118°, may also be
chosen. The hexagonal subcell corresponding to the NiAs (1C) structure is also shown.

Analysis of pyrrhotite - Report Prepared for MIM Exploration

Fig.3. (facing page) The structures of 4C (Fe_7S_8) (Bertaut, 1953) and 6C ($Fe_{11}S_{12}$)
(Koto *et al.*, 1976) pyrrhotites, showing all Fe layers. The dots indicate Fe atoms, open circles
denote vacancies, and the half-filled circles in the 6C superstructure denote vacancy sites with
50% occupation probability. Magnetic moments of Fe atoms in alternate layers are oppositely
directed. Ordering of vacancies onto alternate layers in 4C pyrrhotite produces a nett
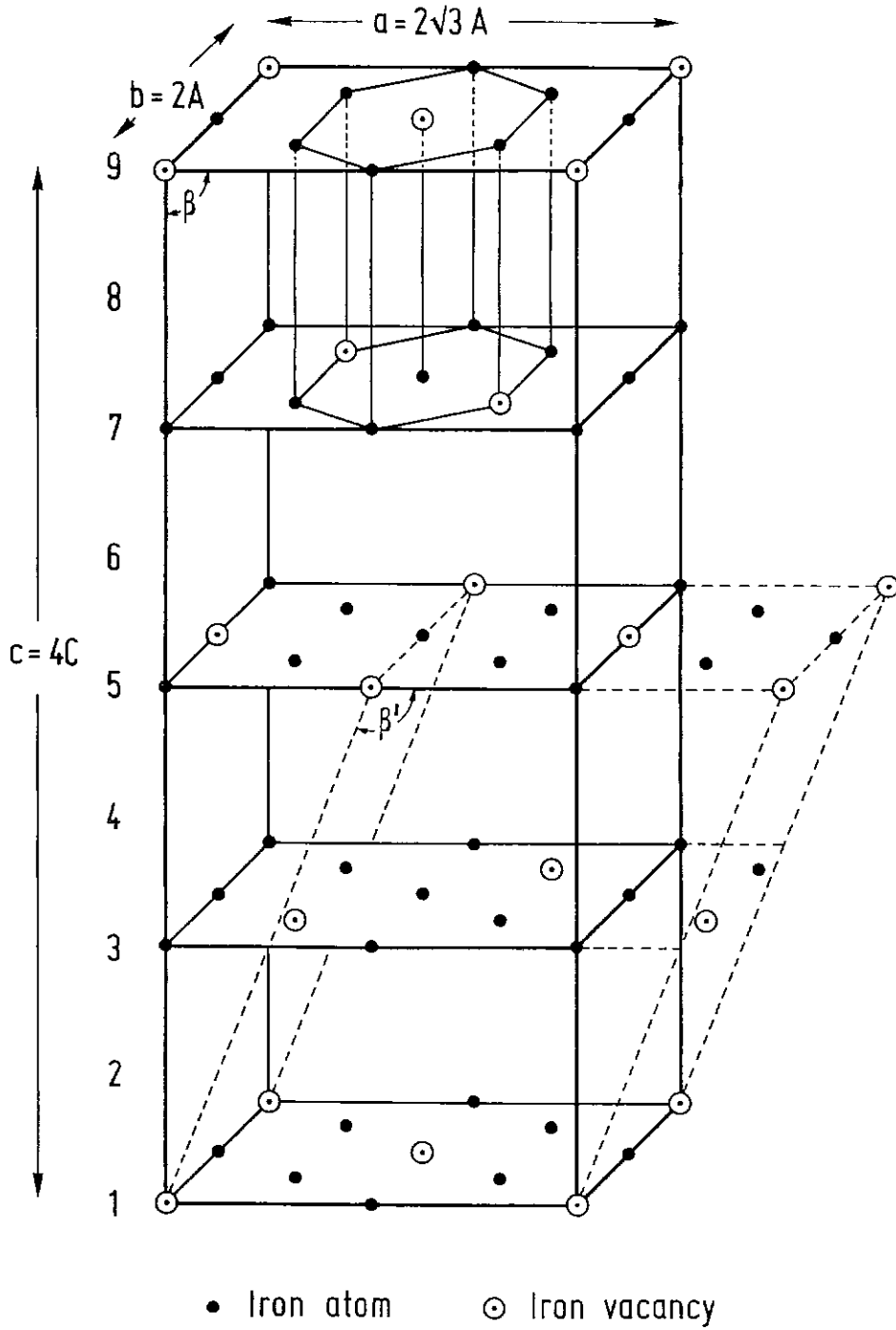ferrimagnetic moment as shown. In 6C pyrrhotite the magnetic moments (not shown) of the
two sublattices (even and odd Fe layers) cancel. Therefore 6C pyrrhotite is antiferromagnetic,
with zero spontaneous magnetisation and a low susceptibility. The ordering of filled (F) and
vacancy (V) layers (which have one in four Fe atoms missing) in 4C pyrrhotite is VFVFVF....
In 6C pyrrhotite it is: vvFvvFvvFvvF..., where v denotes layers with, on average, one Fe atom
in eight missing. Proposed structures for 5C (Fe_9S_{10}) and 11C ($Fe_{10}S_{11}$) pyrrhotites are
FVFFV... and FVFFVFVFFVF... respectively (Schwarz, 1974). These ordering schemes
would explain the antiferromagnetism of 5C and 11C pyrrhotites. However the true structures
of all intermediate pyrrhotites appear to be statistical in nature, arising from antiphase domains
stacked along the c-axis.

Nett spontaneous magnetisation

4C (Fe₇S₈)

6C (Fe₁₁S₁₂)

Magnetic moments of Fe layers

Analysis of pyrrhotite - Report Prepared for MIM Exploration
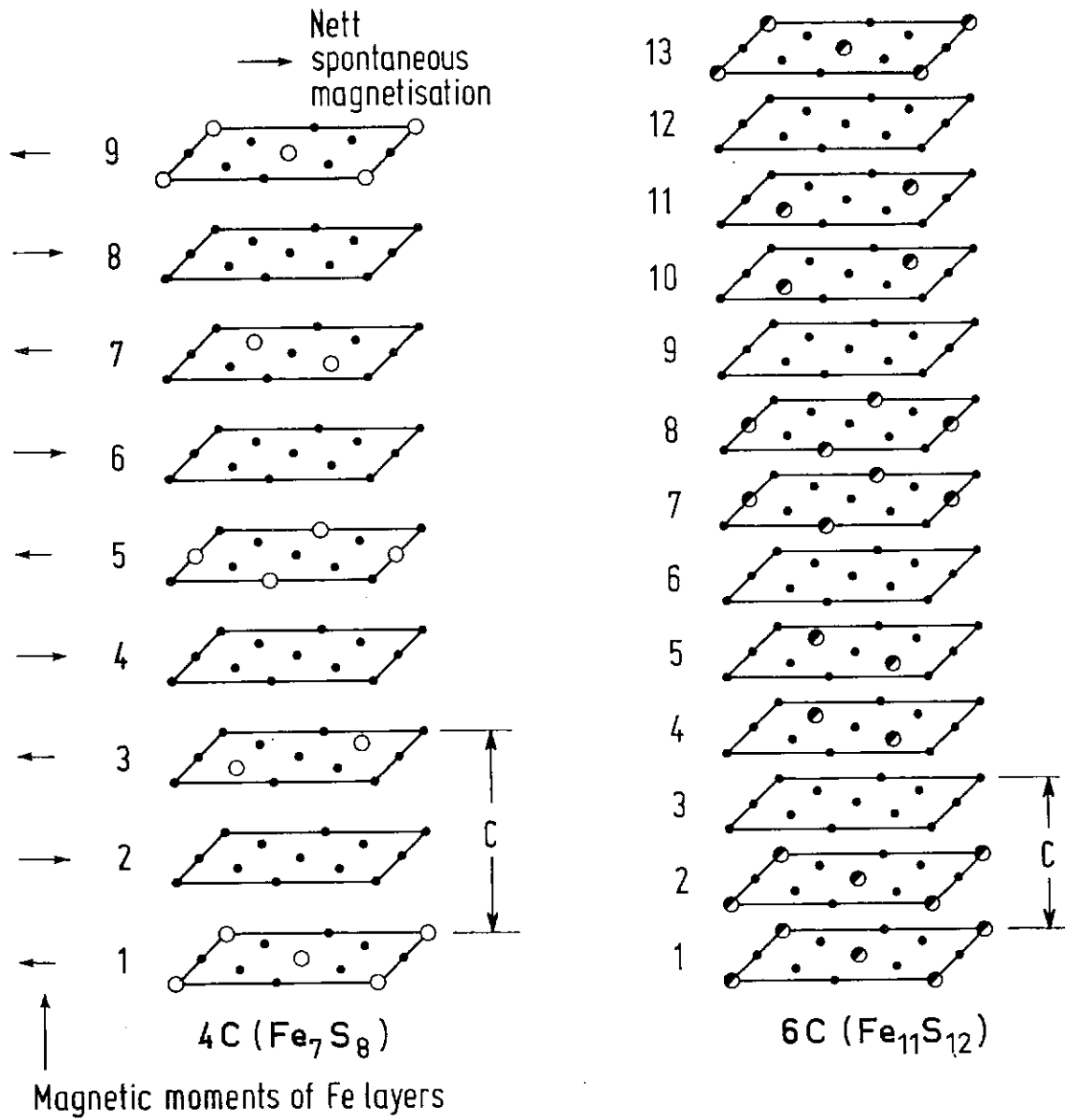
Collectively the nC (n = 5, 11, 12) pyrrhotites should be termed "intermediate pyrrhotites". However they are commonly referred to as "hexagonal pyrrhotite". Although this is crystallographically inaccurate (the apparent hexagonal symmetry is imperfect and is an artefact of stacking of orthorhombic twins, successively rotated by 120°, along the c-axis) and could lead to confusion with 1C high-temperature hexagonal (*sensu stricto*) pyrrhotite, the usage is entrenched. Hereafter in this report "hexagonal pyrrhotite" will be used in the popular sense as a synonym for intermediate pyrrhotite.

Intermediate pyrrhotites with non-integral superstructures (a = 2A; c = NC and a = NA, c = 3C pyrrhotites; N non-integral) are stable at moderately elevated temperatures and have also been found in nature, presumably as quenched metastable phases. The total composition range for intermediate pyrrhotites, including non-integral superstructures, is approximately $0.07 \leq x \leq 0.106$ (47.2 - 48.2 at. % Fe or $\sim Fe_{17}S_{19}$ to $\sim Fe_{13}S_{14}$). The superstructures of all intermediate pyrrhotites, whether apparently integral or non-integral, are probably statistical, arising from stacking of antiphase domains of differing superstructure, each only a few unit cells thick, in a more-or-less disordered sequence along the c-axis.

The magnetic properties of pyrrhotites depend strongly on composition (Schwarz, 1974; Clark, 1983, 1985). There is antiferromagnetic coupling between alternate Fe layers in pyrrhotite. The presence (absence) of a spontaneous magnetisation depends on imperfect (complete) cancellation of the magnetic moments of the two sublattices. Figure 3 shows the vacancy ordering schemes for 4C (monoclinic) pyrrhotite and 6C intermediate pyrrhotite, which explain the ferrimagnetism of 4C pyrrhotite and antiferromagnetism of 6C pyrrhotite. All other stable intermediate pyrrhotites are also antiferromagnetic at room temperature. Thermomagnetic curves reflect a number of physical transitions, including changes in superstructure with temperature, as well as chemical transformations, and are highly diagnostic of composition. Summaries of thermomagnetic characteristics of pyrrhotites can be found in Bleil and Petersen (1982) and Clark (1983, 1985).

Figure 4 (Clark, 1984) shows a phase diagram for the Fe-S system, showing the stability fields of the various pyrrhotite phases. Thermomagnetic curves do not reflect all of the phase boundaries shown, because of sluggish kinetics, at least over the laboratory time scale. In particular, nucleation of pyrite from pyrrhotite involves a major structural change and is negligible over the course of a thermomagnetic run (~ 1 hour). Thus thermomagnetic behaviour of relatively Fe-deficient compositions reflects the loss of magnetic ordering at the Néel point (~325°C), rather than the chemical transformation of vacancy-ordered pyrrhotite to vacancy-disordered 1C hexagonal pyrrhotite + pyrite above 308°C.

Monoclinic pyrrhotite exhibits typical Weiss-type ferromagnetic (*sensu lato*) behaviour, with a steady decrease of spontaneous magnetisation up to the Curie temperature (ferrimagnetic Néel point) at 325°C, above which it is paramagnetic (Fig.5). Intermediate pyrrhotites have zero spontaneous magnetisation at room temperature but, to varying extents depending on composition, start to develop ferrimagnetic superstructures at elevated temperatures. Thus they exhibit "peak-type" thermomagnetic curves, also known as "Λ-type". This behaviour, which is by far most strongly developed in 5C "hexagonal" pyrrhotite (Fe_9S_{10}), is illustrated in Fig.5. Marusak and Mulay (1980) have shown that this composition develops an apparently

non-integral superstructure above ~170°C, with N apparently changing continuously from 5 to 4 between 170°C and 215°C, at which the spontaneous magnetisation attains a maximum. Marusak and Mulay (1980) interpret this mesoscopic non-integral superstructure as arising from stacking of varying proportions of microscopic 5C and 4C (and possibly other integral superstructures) antiphase domains along the c-axis. The apparent non-integral value of N, which shows good agreement between XRD and saturation magnetisation measurements, represents a statistical average over many unit cells.

Above 215°C the spontaneous magnetisation decreases steadily until it vanishes at an apparent Curie point of ~270°C. According to Marusak and Mulay (1980), this transition represents replacement of the 4C superstructure with an antiferromagnetic 2C superstructure. Thus it is not a true ferrimagnetic Curie temperature, but is nevertheless useful for recognition of the Fe_9S_{10} composition.

Hexagonal pyrrhotites that are more Fe-rich than Fe_9S_{10} also exhibit Λ-type curves, but the maximum spontaneous magnetisation is much lower than for Fe_9S_{10} and the thermomagnetic peak is accordingly much more subdued, particularly for smaller values of x. For x < 0.074 the Λ-transition becomes a subtle inflection on the thermomagnetic curve and for x < 0.055 it is altogether absent. The temperature of the Λ-peak, denoted T_γ, and the apparent Curie point both decrease with decreasing x.

Schwarz (1974) used high-field thermomagnetic (saturation magnetisation versus temperature) curves to estimate monoclinic and 5C hexagonal pyrrhotite contents of sulphide ores. Figures 6-17 show high-field (7600 Oe = 0.76 T) thermomagnetic curves for subsamples from the each of the ore samples, obtained using the VFTB. Monoclinic pyrrhotite (Curie temperature ~330°C) is present in all samples, except SC13 and W1. A number of samples (L2, MI56B, MI56C, RB03, RB09) exhibit clear Λ peaks, superimposed on characteristic Weiss-type curves due to monoclinic pyrrhotite. Thus these samples clearly contain both monoclinic and 5C hexagonal pyrrhotites. The relative prominence of the Λ peak gives a semi-quantitative indication of the relative proportions of the two pyrrhhotite phases. For example, it is evident that RB03 contains a much higher proportion of 5C pyrrhotite, relative to monoclinic pyrrhotite, than does RB09.

Schwarz (1974) used the form of these curves to estimate concentratations of the two phases, but the method described in the next section is more sensitive to the presence of minor amounts of 5C pyrrhotite and is more accurate overall. This point is exemplified by samples MI11, MI20 and MI55B, which contain significant amounts of 5C hexagonal pyrrhotite (4-10 vol. %), but do not exhibit a clear Λ peak, due to the dominance of monoclinic pyrrhotite.

Fig.4. (facing page) Phase diagram for the central part of the Fe-S system below 350°C (after Power and Fine, 1976). Sluggish kinetics preclude significant nucleation of pyrite during a thermomagnetic run (~1 hour). Thus monoclinic pyrrhotite retains the 4C structure during thermomagnetic analysis, losing its ferrimagnetism only at the spin-disordering temperature (the Néel point or β transition: ~325°C). 5C "hexagonal" pyrrhotite develops a non-integral NC superstructure above ~170°, attaining maximum ferrimagnetism when $N = 4$ at ~215°C. Thereafter, N decreases gradually to 2 at the apparent Curie temperature (~270°C). "Hexagonal" pyrrhotites with $x < 0.1$ also develop non-integral superstructures above ~110-150°C, but the proportion of 4C unit cells within the mesoscopically non-integral superstructures is much less than that of 5C ($x = 0.1$) pyrrhotite. Thus the ferrimagnetism of these compositions around the Λ-peak (150°C for $x = 0.058$, up to 215°C for $x = 0.091$: $Fe_{10}S_{11}$) is much weaker than that of Fe_9S_{10}.

Analysis of pyrrhotite - Report Prepared for MIM Exploration

Magnetic β transition (Néel point)

308°
262°
254°
~75°

IC + Pyrite

MC (non-integral, "hexagonal") pyrrhotite + pyrite

NA (non-integral, "hexagonal") pyrrhotite + pyrite

Monoclinic pyrrhotite (Po$_m$) + pyrite (Py)

Greigite

Fe$_3$S$_4$

Smythite + Pyrite (Py)

Smythite + Monoclinic pyrrhotite

Fe$_9$S$_{11}$

Fe$_7$S$_8$

Fe$_9$S$_{10}$

Fe$_{10}$S$_{11}$

Fe$_{11}$S$_{12}$

IC (hexagonal pyrrhotite with NiAs structure)

MC

NA

NA + Po$_m$

Po$_m$ (4C)

NC + Po$_m$

NC (non-integral, "hexagonal") pyrrhotite

nC + 4C (Po$_m$)

nC
11C 5C
6C

α transition

2C + IC

2C (troilite) + nC (intermediate pyrrhotite)

Atomic % Fe

Temperature, °C

300
200
100
0

50
49
48
47
46
45
44
43
42

FeS

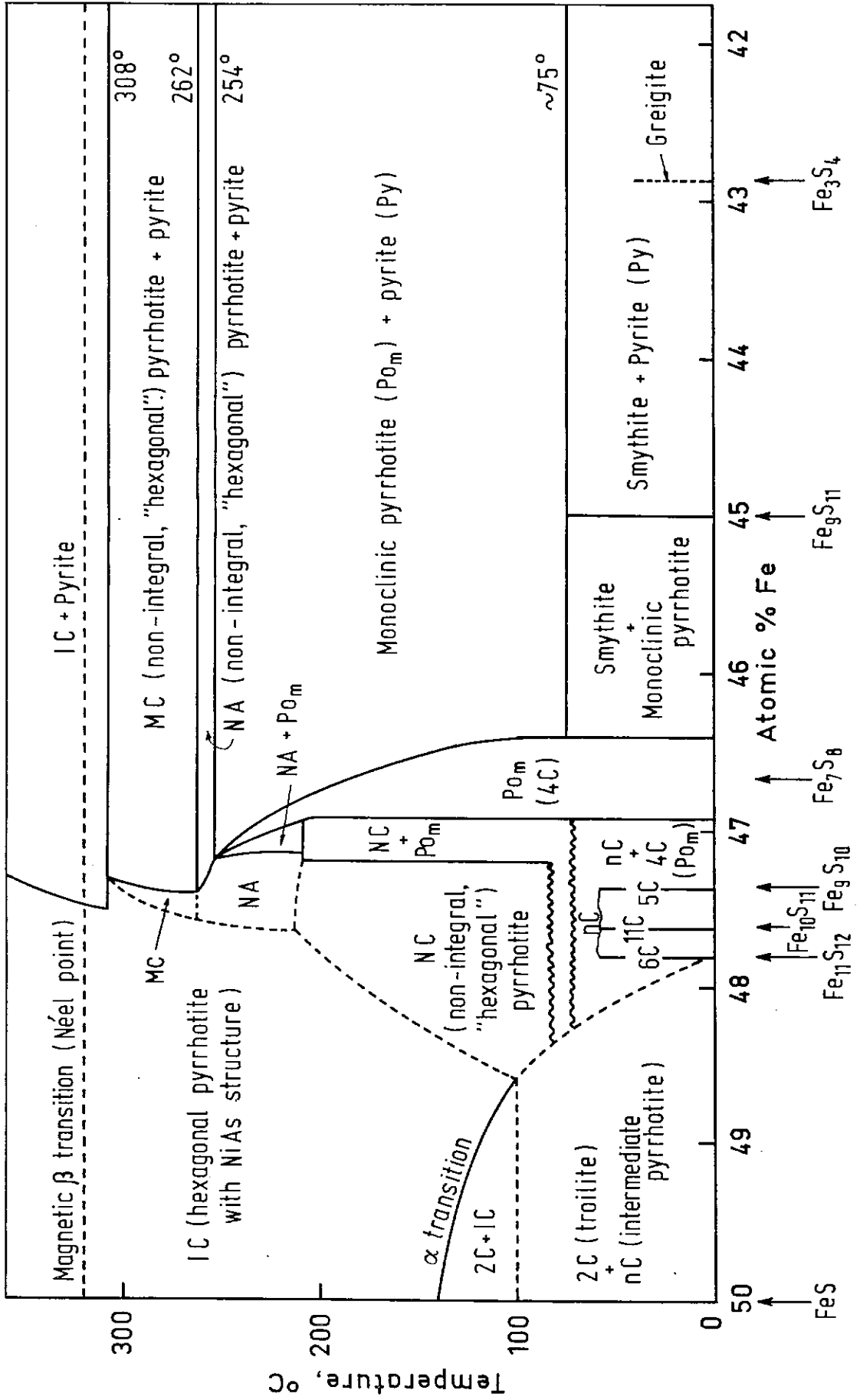Analysis of pyrrhotite - Report Prepared for MIM Exploration

Fig.5. (facing page) High field thermomagnetic (saturation magnetisation vs temperature) curves for 4C monoclinic pyrrhotite (Fe_7S_8) and 5C hexagonal pyrrhotite (Fe_9S_{10}), showing Weiss-type and peak-type behaviour respectively. 5C pyrrhotite is antiferromagnetic at room temperature, becomes ferrimagnetic at the so-called Haraldsen point, T_H, also known as the "anti-Curie point", and reverts to antiferromagnetism at T_C (after Schwarz and Vaughn, 1972).
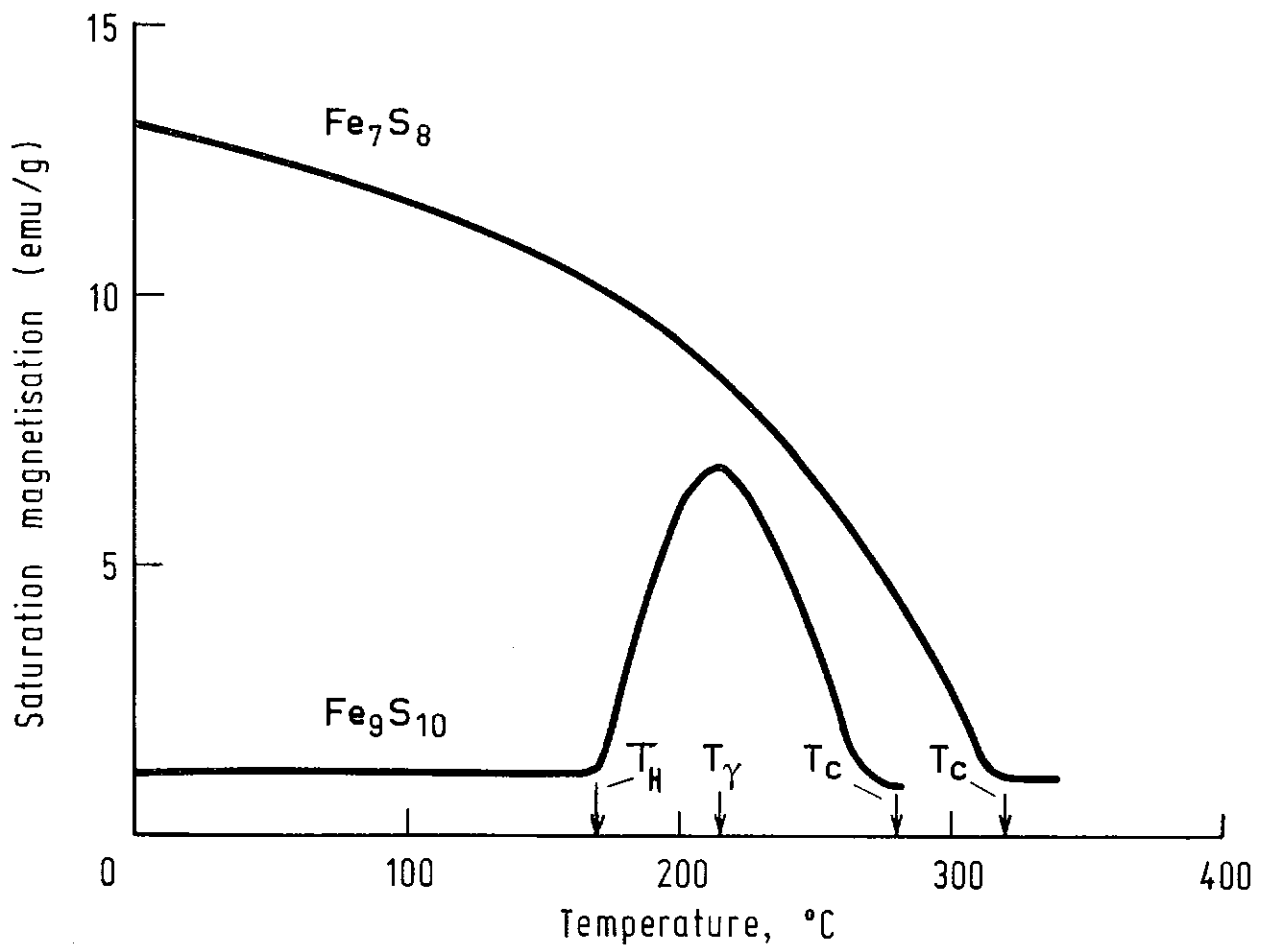
Fig.6. (facing page) High field thermomagnetic (saturation magnetisation vs temperature) curve for a subsample of pyrrhotite-bearing ore L2. In this, and all subsequent thermomagnetic curves, specific magnetisation is given in mAm^2/kg (10^{-3} emu/g). The curve indicates mixed 4C monoclinic and 5C hexagonal pyrrhotite, with compositions of ~ Fe_7S_8 and ~Fe_9S_{10} respectively, which have apparent Curie temperatures of ~270°C and ~330°C as shown. The magnetisation above 330°C is due to the presence of minor magnetite (T_C = 580°C), which is augmented by extra magnetite, especially evident in the cooling curve, produced by oxidation of iron sulphides during heating to 700°C. The cooling rate is sufficiently rapid to essentially quench the ferrimagnetic superstructure developed by the Fe_9S_{10} composition between 270°C and 170°C, so the Λ-peak is not reversible.

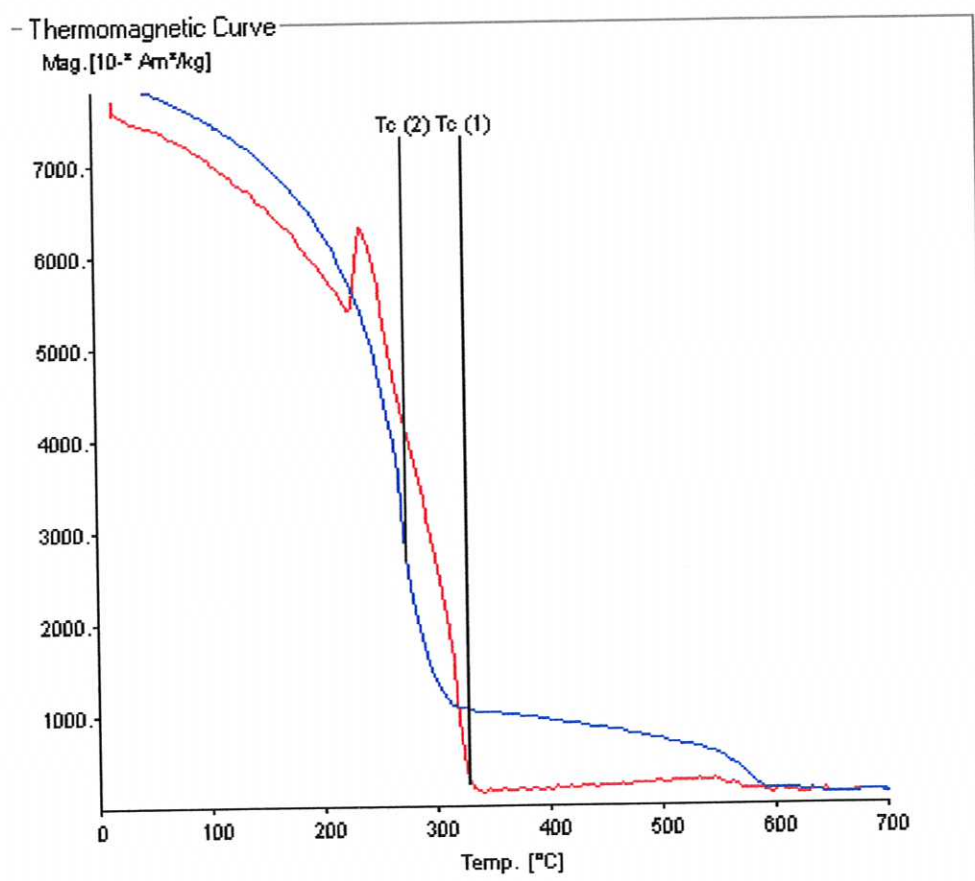Analysis of pyrrhotite - Report Prepared for MIM Exploration

Fig. 7. (facing page) High field thermomagnetic (saturation magnetisation vs temperature) curve for a subsample of pyrrhotite-bearing ore MI01. Specific magnetisation is given in mAm²/kg (10^{-3} emu/g). The curve indicates predominantly 4C monoclinic pyrrhotite with a Curie temperature of 330°C. As shown by high temperature hysteresis data, the normalised curve between 170°C and 270°C lies slightly above the curve for pure monoclinic pyrrhotite, due to the presence of minor 5C pyrrhotite, but this is not readily observable in the thermomagnetic curve. The magnetisation above 330°C is due to paramagnetism, plus the presence of traces of magnetite (T_C = 580°C), which is augmented by extra magnetite, especially evident in the cooling curve, produced by oxidation of iron sulphides during heating to 600°C.
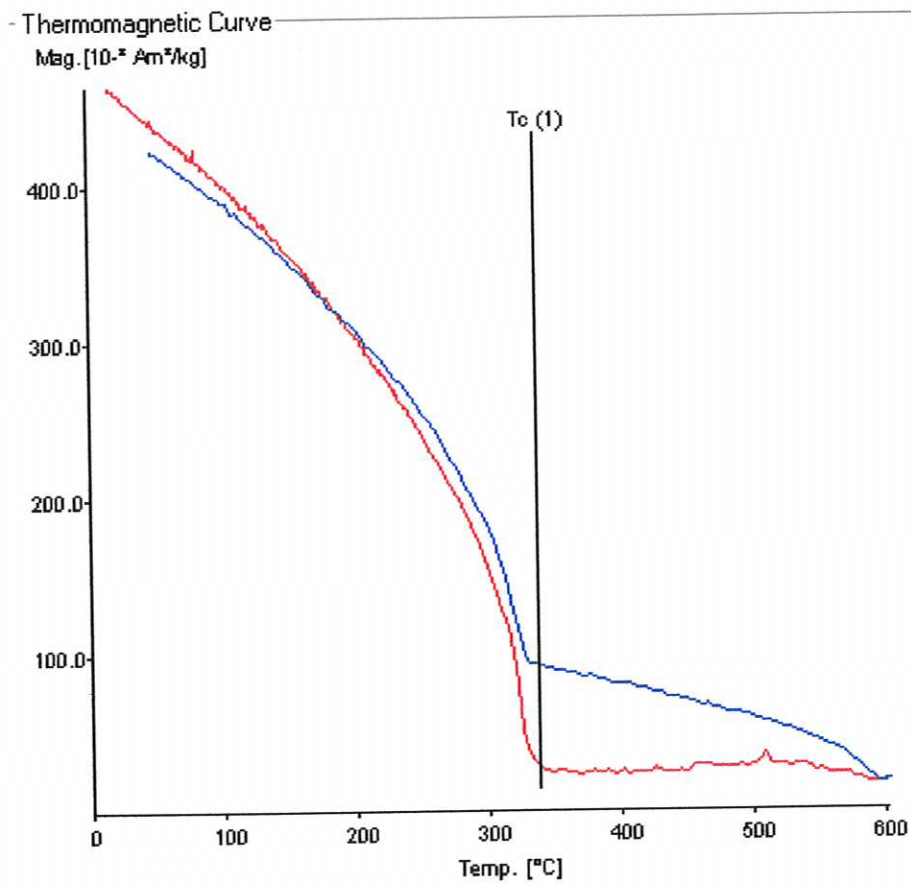
Thermomagnetic Curve

Mag.[10⁻³ Am²/kg]

Analysis of pyrrhotite - Report Prepared for MIM Exploration

Fig.8. (facing page) High field thermomagnetic (saturation magnetisation vs temperature) curve for a subsample of pyrrhotite-bearing ore MI11. Specific magnetisation is given in mAm^2/kg (10^{-3} emu/g). The curve indicates predominantly 4C monoclinic with a Curie temperature of 330°C. As shown by high temperature hysteresis data, the normalised curve between 170°C and 270°C lies slightly above the curve for pure monoclinic pyrrhotite, due to the presence of minor 5C pyrrhotite, but this is not readily observable in the thermomagnetic curve. The magnetisation above 330°C is due to the presence of minor magnetite (T_C = 580°C), some of which breaks down during heating to 600°C.

Analysis of pyrrhotite - Report Prepared for MIM Exploration

Fig.9. (facing page) High field thermomagnetic (saturation magnetisation vs temperature) curve for a subsample of pyrrhotite-bearing ore MI19. Specific magnetisation is given in mAm²/kg (10^{-3} emu/g). The curve indicates predominantly 4C monoclinic pyrrhotite with a Curie temperature of 330°C. As shown by high temperature hysteresis data, the normalised curve between 170°C and 270°C lies slightly above the curve for pure monoclinic pyrrhotite, due to the presence of minor 5C pyrrhotite, but this is not readily observable in the thermomagnetic curve. The magnetisation above 330°C is due to paramagnetism, plus the presence of traces of magnetite (T_C = 580°C), which is produced by oxidation of iron sulphides during heating to from 400°C to 600°C. The noisy curves are due to the weakness of the magnetisation.

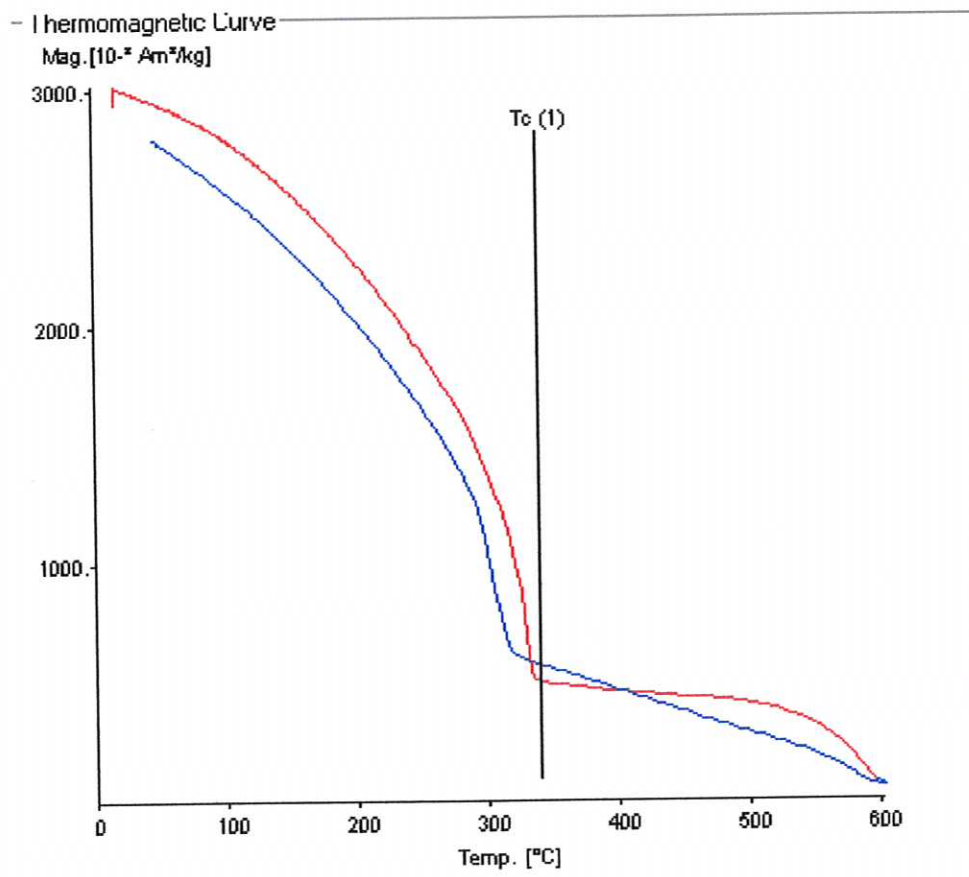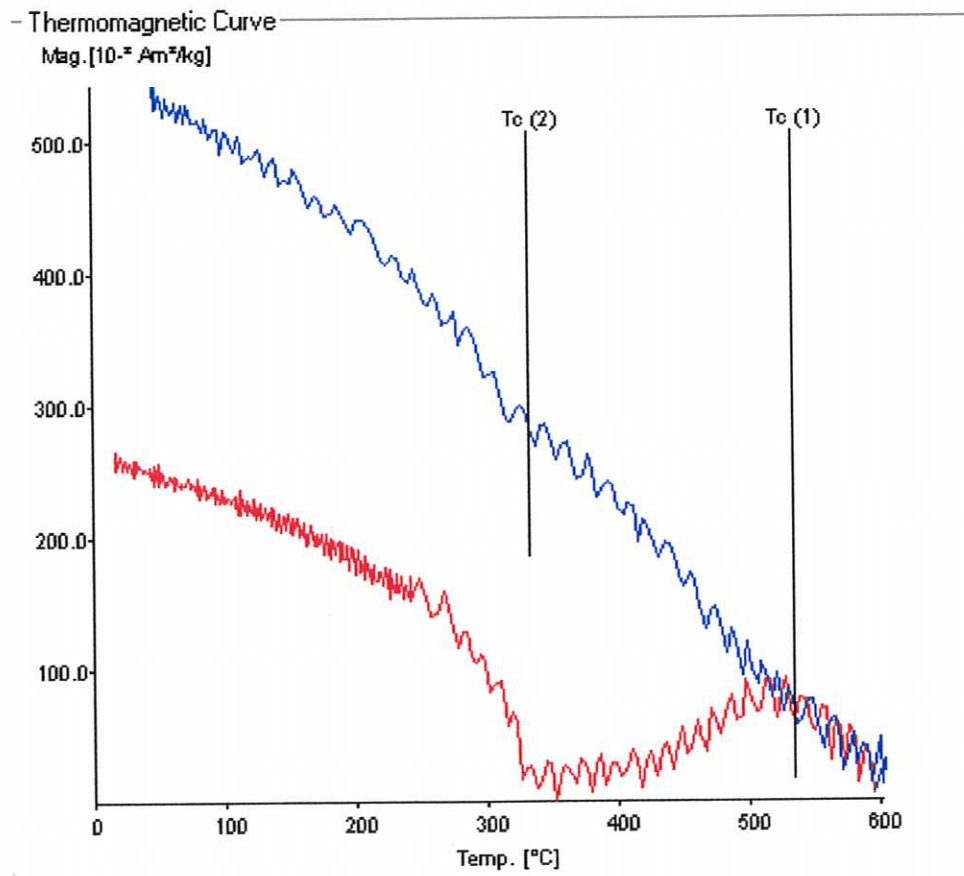Analysis of pyrrhotite - Report Prepared for MIM Exploration

Fig.10. (facing page) High field thermomagnetic (saturation magnetisation vs temperature) curve for a subsample of pyrrhotite-bearing ore MI20. Specific magnetisation is given in mAm²/kg (10^{-3} emu/g). The curve indicates predominantly 4C monoclinic pyrrhotite with a Curie temperature of 330°C. As shown by high temperature hysteresis data, the normalised curve between 170°C and 270°C lies slightly above the curve for pure monoclinic pyrrhotite, due to the presence of minor 5C pyrrhotite, but this is not readily observable in the thermomagnetic curve. The magnetisation above 330°C is due to paramagnetism, plus the presence of traces of magnetite ($T_C = 580$°C), which is augmented by extra magnetite, especially evident in the cooling curve, produced by oxidation of iron sulphides during heating to 600°C.

Analysis of pyrrhotite - Report Prepared for MIM Exploration

Fig.11. (facing page) High field thermomagnetic (saturation magnetisation vs temperature) curve for a subsample of pyrrhotite-bearing ore MI55B. Specific magnetisation is given in mAm^2/kg (10^{-3} emu/g). The curve indicates predominantly 4C monoclinic pyrrhotite with a Curie temperature of 330°C. As shown by high temperature hysteresis data, the normalised curve between 170°C and 270°C lies slightly above the curve for pure monoclinic pyrrhotite, due to the presence of minor 5C pyrrhotite, but this is not readily observable in the thermomagnetic curve. The magnetisation above 330°C is due to paramagnetism, plus the presence of traces of magnetite (T_C = 580°C), which is augmented by extra magnetite, especially evident in the cooling curve, produced by oxidation of iron sulphides during heating to 600°C.
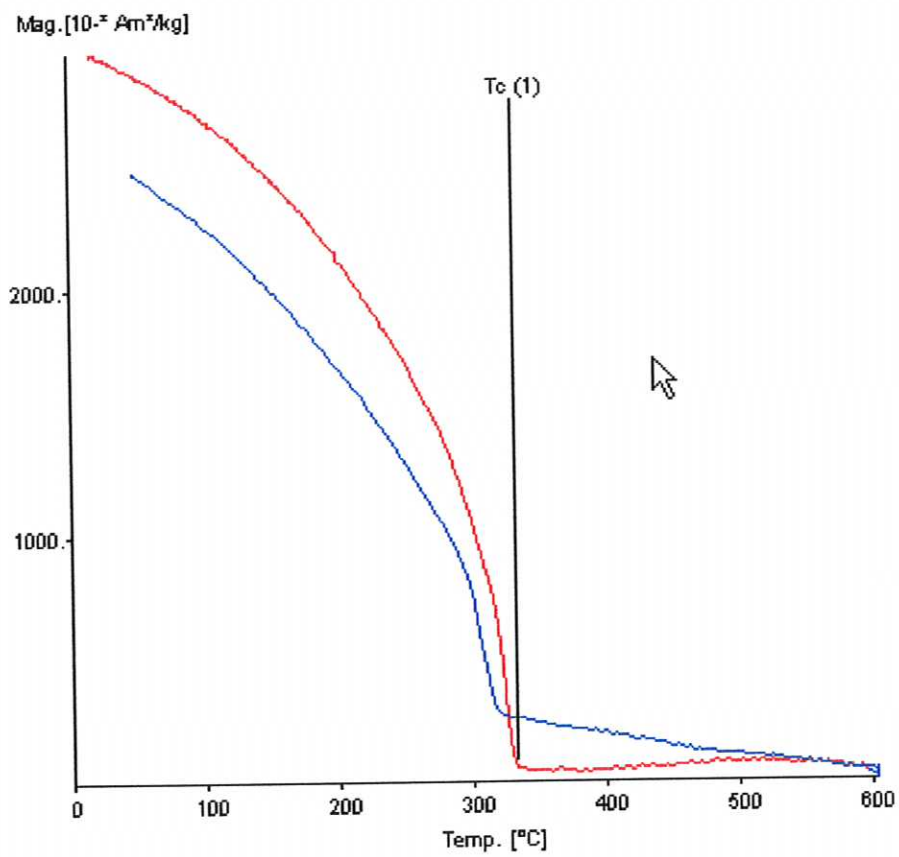
Mag.[10⁻² Am²/kg]

Tc (1)

2000.

1000.

0   100   200   300   400   500   600

Temp. [°C]

Analysis of pyrrhotite - Report Prepared for MIM Exploration

Fig.12. (facing page) High field thermomagnetic (saturation magnetisation vs temperature) curve for a subsample of pyrrhotite-bearing ore MI56B. Specific magnetisation is given in mAm^2/kg (10^{-3} emu/g). The curve indicates mixed 4C monoclinic and 5C hexagonal pyrrhotite, with compositions of ~ Fe_7S_8 and ~Fe_9S_{10} respectively, which have apparent Curie temperatures of ~270°C and ~330°C. The magnetisation above 330°C is due to the presence of minor magnetite ($T_C = 580$°C), which is augmented by extra magnetite, especially evident in the cooling curve, produced by oxidation of iron sulphides during heating to 700°C. The cooling rate is sufficiently rapid to essentially quench the ferrimagnetic superstructure developed by the Fe_9S_{10} composition between 270°C and 170°C, so the Λ-peak is not reversible.

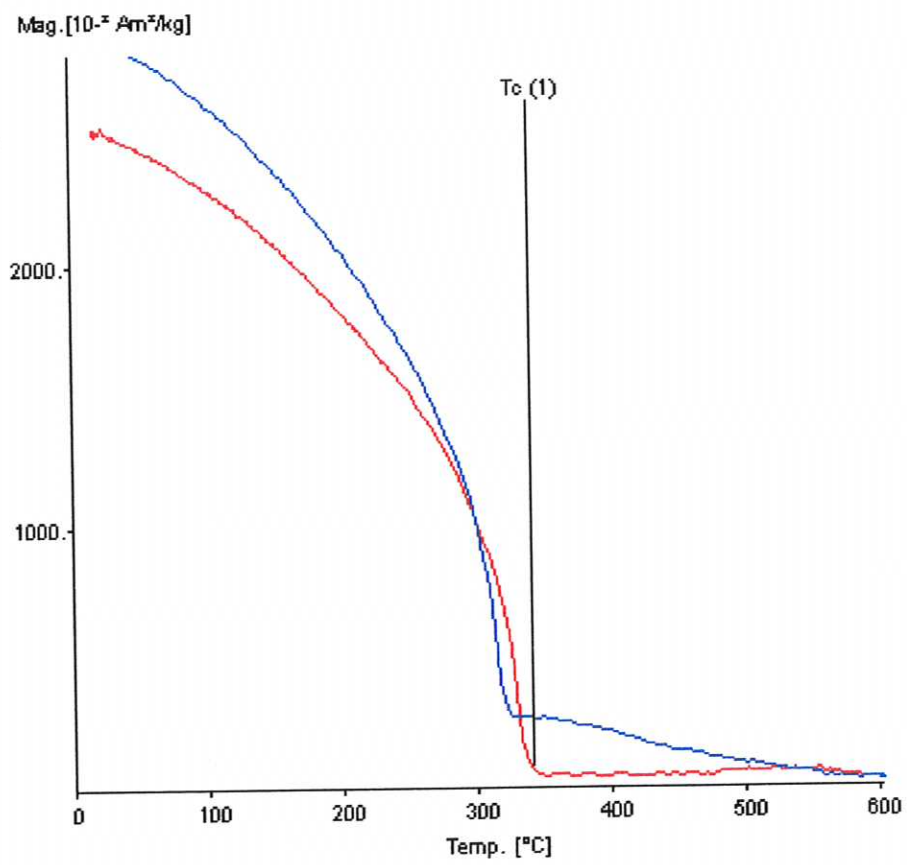Analysis of pyrrhotite - Report Prepared for MIM Exploration

Fig.13. (facing page) High field thermomagnetic (saturation magnetisation vs temperature) curve for a subsample of pyrrhotite-bearing ore MI56C. Specific magnetisation is given in mAm^2/kg (10^{-3} emu/g). The curve indicates mixed 4C monoclinic and 5C hexagonal pyrrhotite, with compositions of ~ Fe_7S_8 and ~Fe_9S_{10} respectively, which have apparent Curie temperatures of ~270°C and ~330°C. The magnetisation above 330°C is due to the presence of minor magnetite (T_C = 580°C), which is augmented by extra magnetite, especially evident in the cooling curve, produced by oxidation of iron sulphides during heating to 700°C. The cooling rate is sufficiently rapid to essentially quench the ferrimagnetic superstructure developed by the Fe_9S_{10} composition between 270°C and 170°C, so the Λ-peak is not reversible.
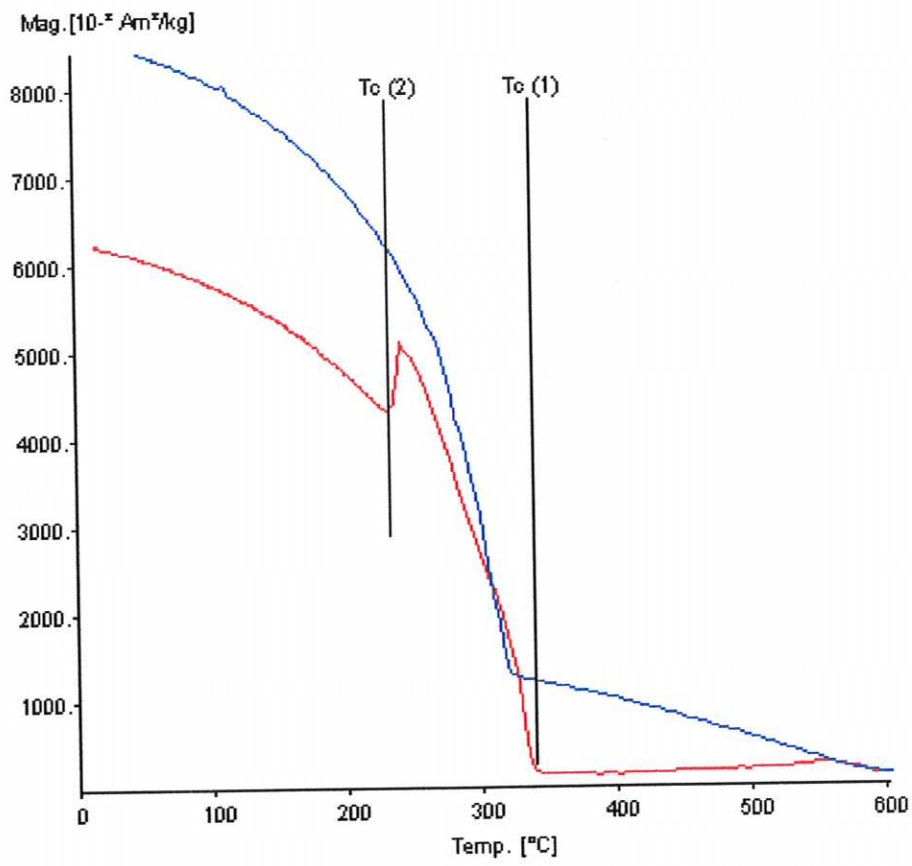
Analysis of pyrrhotite - Report Prepared for MIM Exploration

Fig.14. (facing page) High field thermomagnetic (saturation magnetisation vs temperature) curve for a subsample of pyrrhotite-bearing ore RB03. Specific magnetisation is given in mAm^2/kg (10^{-3} emu/g). The curve indicates minor 4C monoclinic and more abundant 5C hexagonal pyrrhotite, with compositions of ~ Fe_7S_8 and ~Fe_9S_{10} respectively, which have apparent Curie temperatures of ~270°C and ~330°C. The magnetisation above 330°C is due to the presence of minor magnetite (T_C = 580°C), which is augmented by extra magnetite, especially evident in the cooling curve, produced by oxidation of iron sulphides during heating to 700°C. The cooling rate is sufficiently rapid to essentially quench the ferrimagnetic superstructure developed by the Fe_9S_{10} composition between 270°C and 170°C, so the Λ-peak is not reversible.

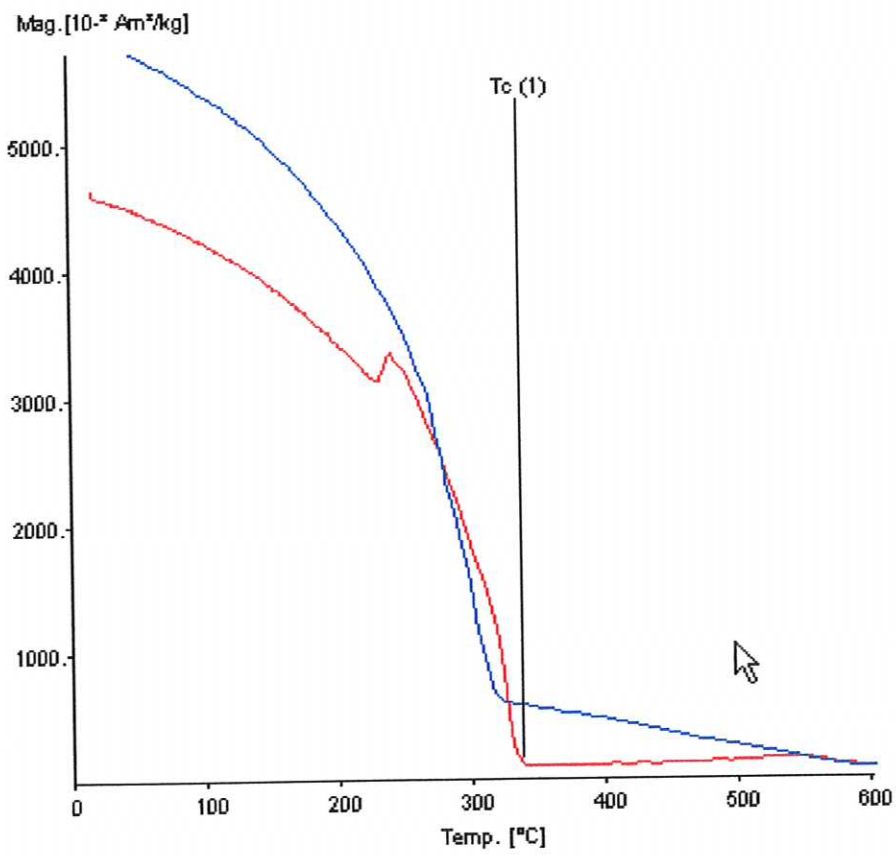Analysis of pyrrhotite - Report Prepared for MIM Exploration

Fig.15. (facing page) High field thermomagnetic (saturation magnetisation vs temperature) curve for a subsample of pyrrhotite-bearing ore RB09. Specific magnetisation is given in mAm^2/kg (10^{-3} emu/g). The curve indicates minor mixed 4C monoclinic and 5C hexagonal pyrrhotite, with compositions of ~ Fe_7S_8 and ~Fe_9S_{10} respectively, which have apparent Curie temperatures of ~270°C and ~330°C. The magnetisation above 330°C is due to the presence of magnetite (T_C = 580°C), which dominates the magnetisation of the sample. Magnetite is neither created nor destroyed during heating of this sample. The cooling rate is sufficiently rapid to essentially quench the ferrimagnetic superstructure developed by the Fe_9S_{10} composition between 270°C and 170°C, so the Λ-peak is not reversible.

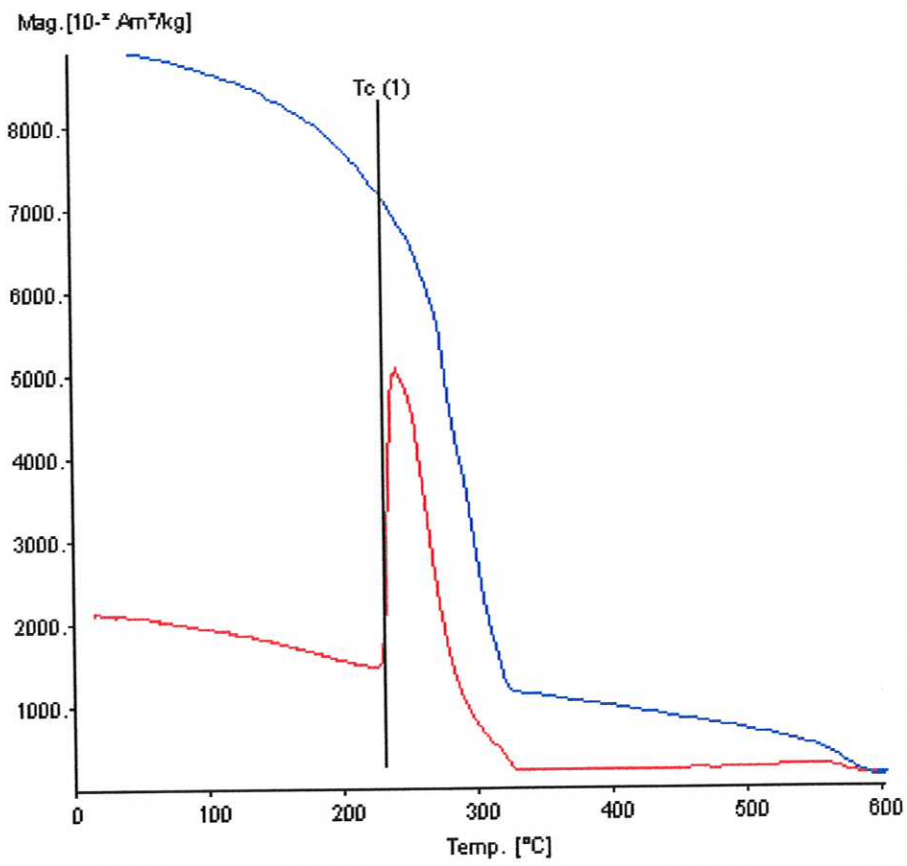Analysis of pyrrhotite - Report Prepared for MIM Exploration

Fig.16. (facing page) High field thermomagnetic (saturation magnetisation vs temperature) curve for a subsample of pyrrhotite-bearing ore SC13. Specific magnetisation is given in mAm^2/kg (10^{-3} emu/g). The curve indicates minor 5C hexagonal pyrrhotite, with composition $\sim Fe_9S_{10}$, which has an apparent Curie temperatures of $\sim 270°C$. The magnetisation above $330°C$ is due to the presence of magnetite ($T_C = 580°C$), which dominates the magnetisation of the sample. Small amounts of magnetite were created during heating of this sample. The cooling rate is sufficiently rapid to essentially quench the ferrimagnetic superstructure developed by the Fe_9S_{10} composition between $270°C$ and $170°C$, so the Λ-peak is not reversible.

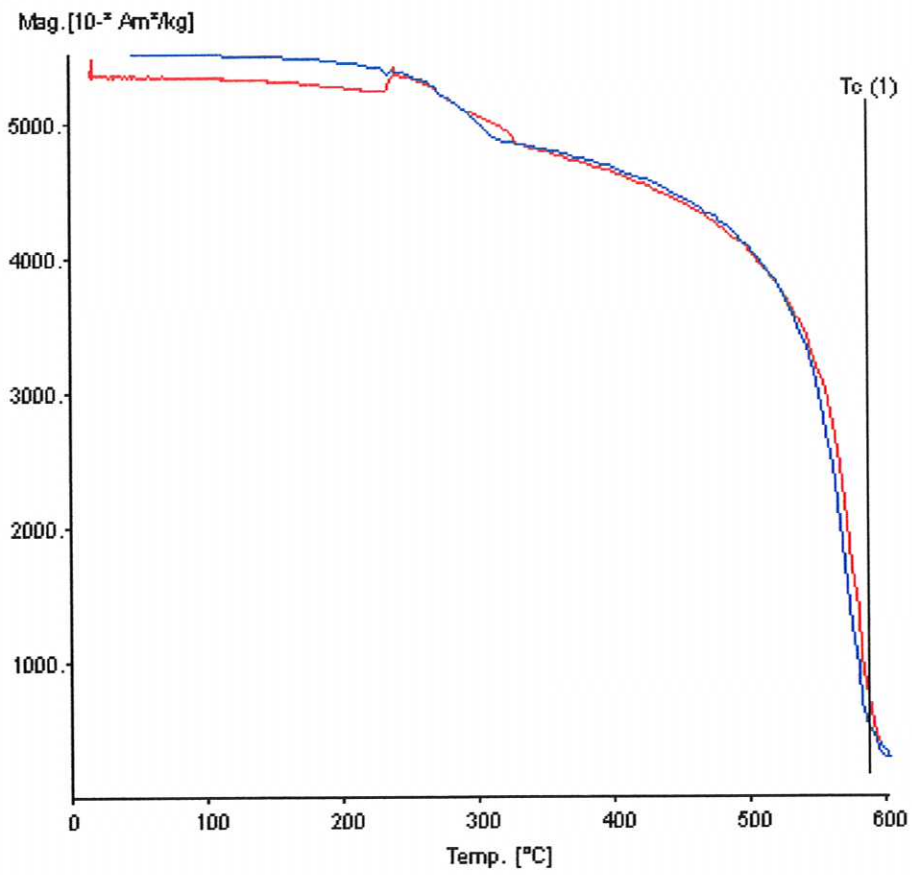Analysis of pyrrhotite - Report Prepared for MIM Exploration
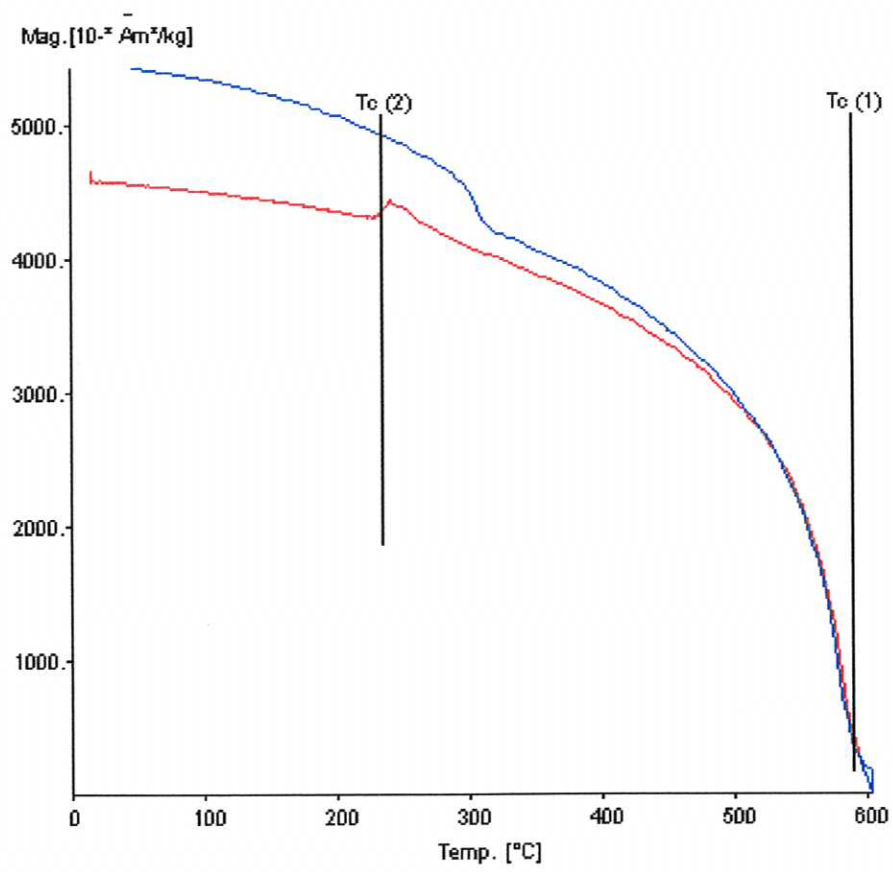
Fig.17. (facing page) High field thermomagnetic (saturation magnetisation vs temperature) curve for a subsample of pyrrhotite-bearing ore W1. Specific magnetisation is given in mAm^2/kg (10^{-3} emu/g). The curve indicates that this massive pyrrhotite contains negligible amounts of either monoclinic or 5C hexagonal pyrrhotite. The absence of any Λ-peak shows that the pyrrhotite must be considerably more Fe-rich than 5C pyrrhotite. The magnetisation above 330°C is due to the presence of traces of magnetite ($T_C = 580$°C), which dominates the magnetisation of the sample. Additional magnetite is created during heating of this sample.

Analysis of pyrrhotite - Report Prepared for MIM Exploration
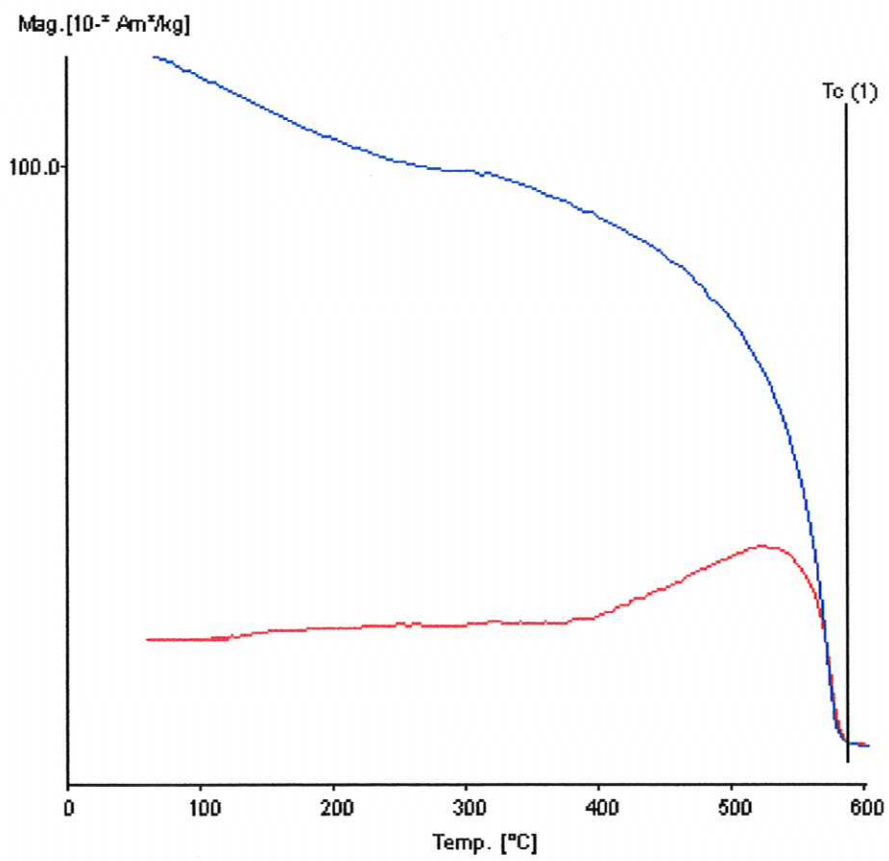
Fig.18. (following pages) Thermal demagnetisation curves for high, intermediate and low coercivity components (z, y, x-components respectively) imparted to specimens of the pyrrhotite-bearing ores, based on the method of Lowrie (1990).

Analysis of pyrrhotite - Report prepared for MIM Exploration.

Analysis of pyrrhotite - Report prepared for MIM Exploration.
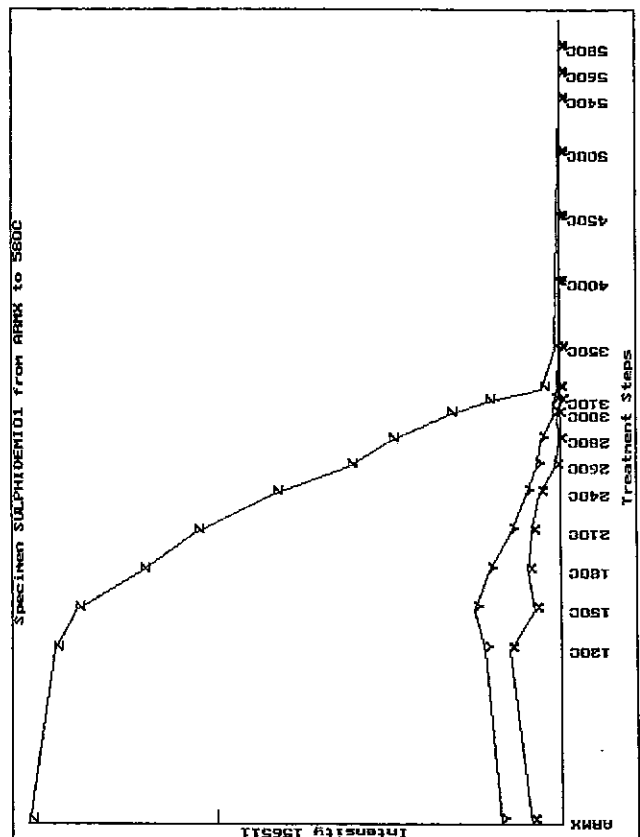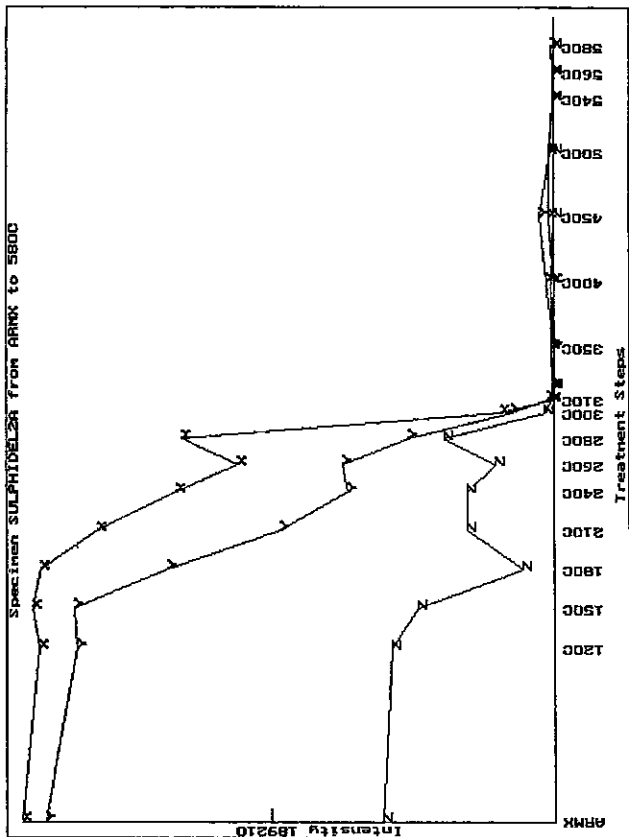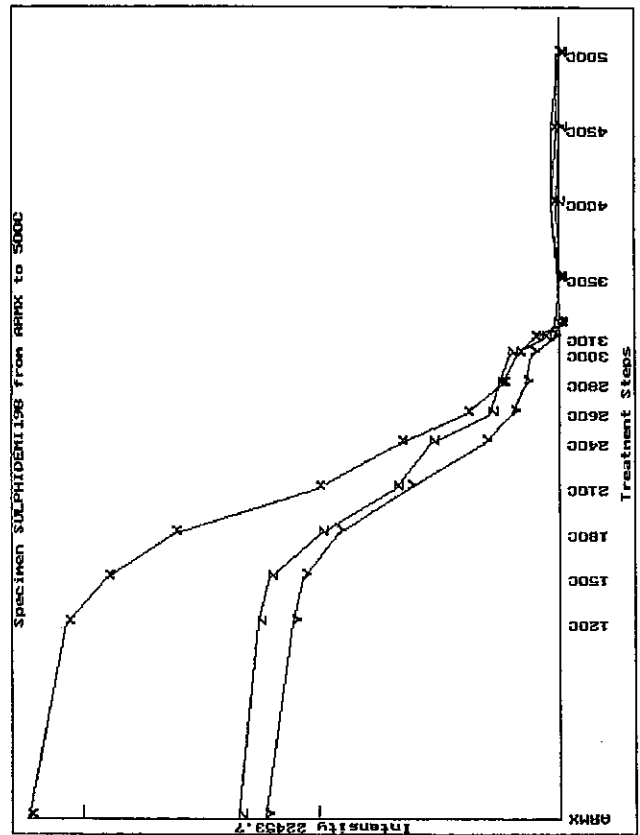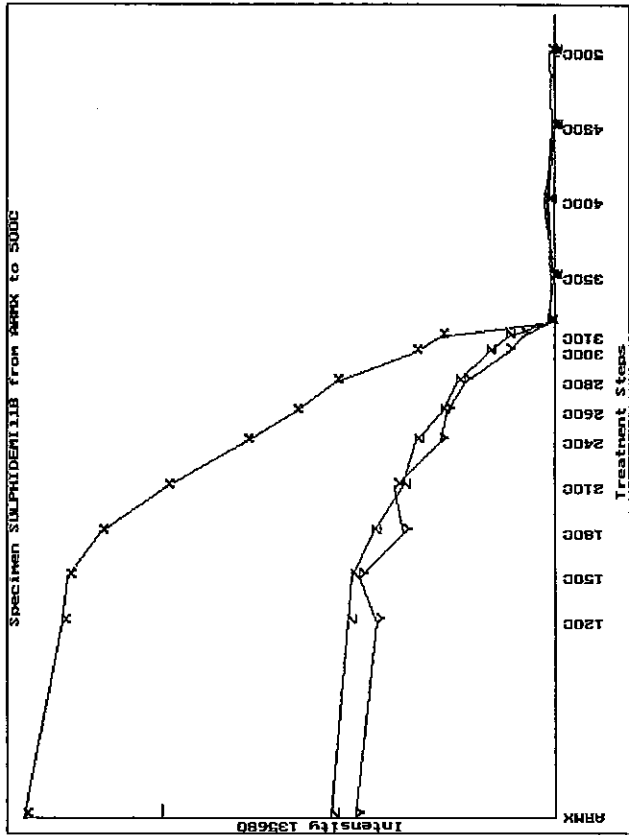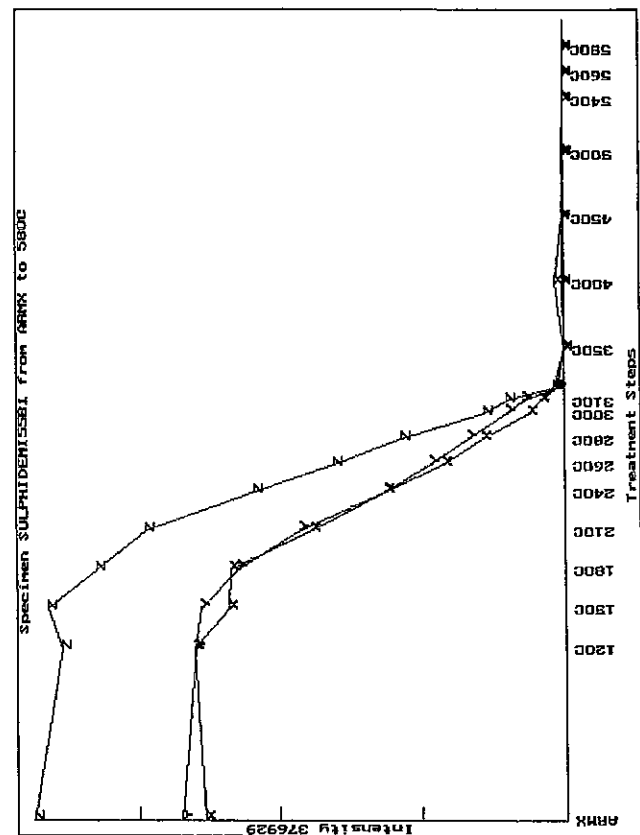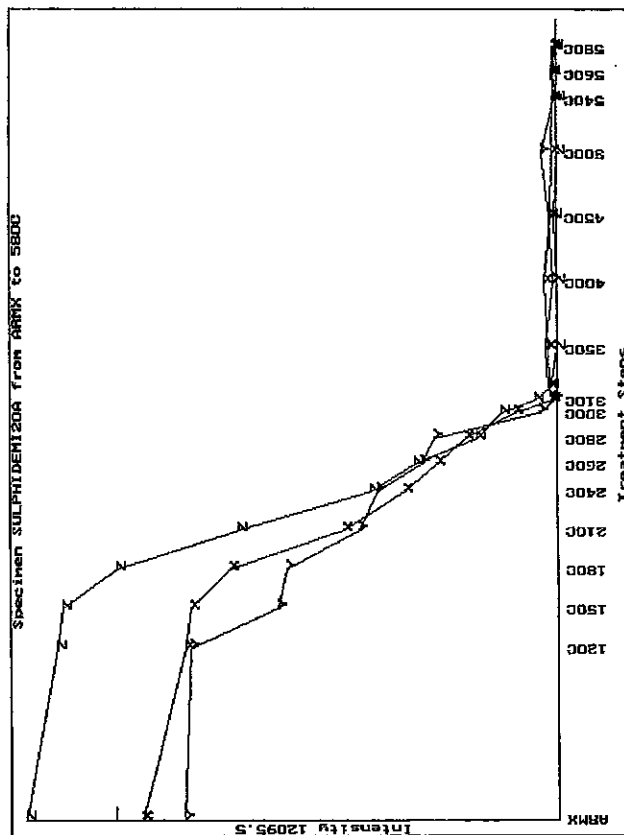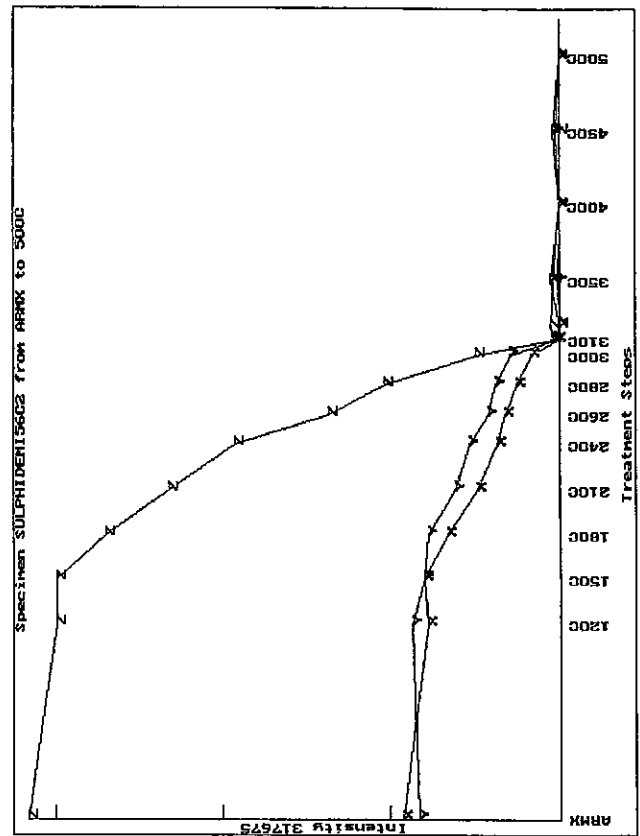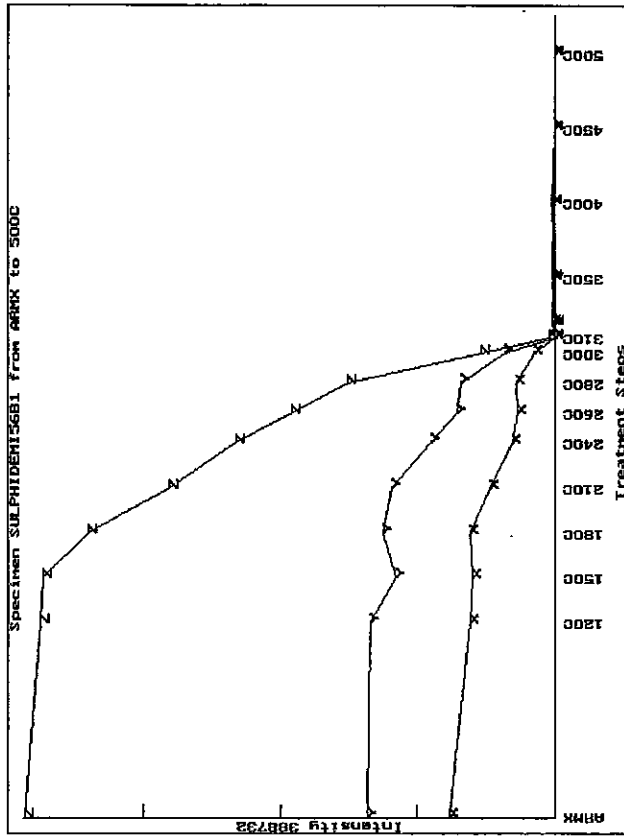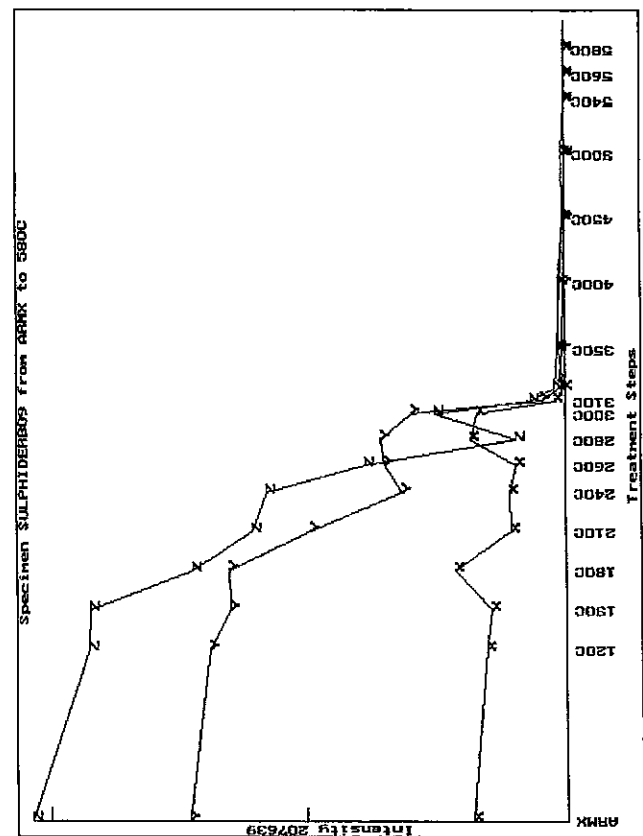
Analysis of pyrrhotite - Report prepared for MIM Exploration.

The magnetic properties of the SC13 sample are dominated by magnetite. Pyrrhotite is abundant in this sample, but the thermomagnetic curve suggests that it is predominantly hexagonal pyrrhotite. The W1 sample is very weakly magnetic, although it contains abundant pyrrhotite. Its thermomagnetic curve shows that W1 contains neither monoclinic nor 5C hexagonal pyrrhotite. The pyrrhotite in W1 is considerably more Fe-rich than 5C pyrrhotite, as it shows little evidence of a Λ-transition. In fact some of the iron sulphide in W1 is probably troilite. The weak magnetisation of W1 is dominated by trace amounts of magnetite (Curie point 580°C). Above ~400°C additional magnetite is created by oxidation of the hexagonal pyrrhotite ± troilite, so that the cooling curve from 600°C is considerably above the initial heating curve.

It is a feature of pyrrhotite-bearing ores generally that some magnetite is created during heating in air to temperatures above 400°C, with greater quantities produced at even higher temperatures. Thus, with the exception of sample MI11, all the thermomagnetic curves show some evidence of irreversibility due to creation of magnetite during the heating cycle. The oxidation of monoclinic and 5C hexagonal pyrrhotites respectively to magnetite can be written as:

$$3Fe_7S_8 + 38O_2 \rightarrow 7Fe_3O_4 + 24SO_2$$

$$2Fe_9S_{10} + 32O_2 \rightarrow 6Fe_3O_4 + 20SO_2 .$$

For sample MI11, on the other hand, some magnetite initially present is destroyed after heating to 600°C. This suggests that the presence of some other, even more easily oxidised, sulphide phase(s) in the ore has consumed oxygen and produced a more reducing environment at high temperatures. It is possible that, in such an environment, some of the magnetite has reduced monoclinic pyrrhotite to hexagonal pyrrhotite according to the nominal reaction:

$$24Fe_7S_8 + Fe_3O_4 \rightarrow 19Fe_9S_{10} + 2SO_2 .$$
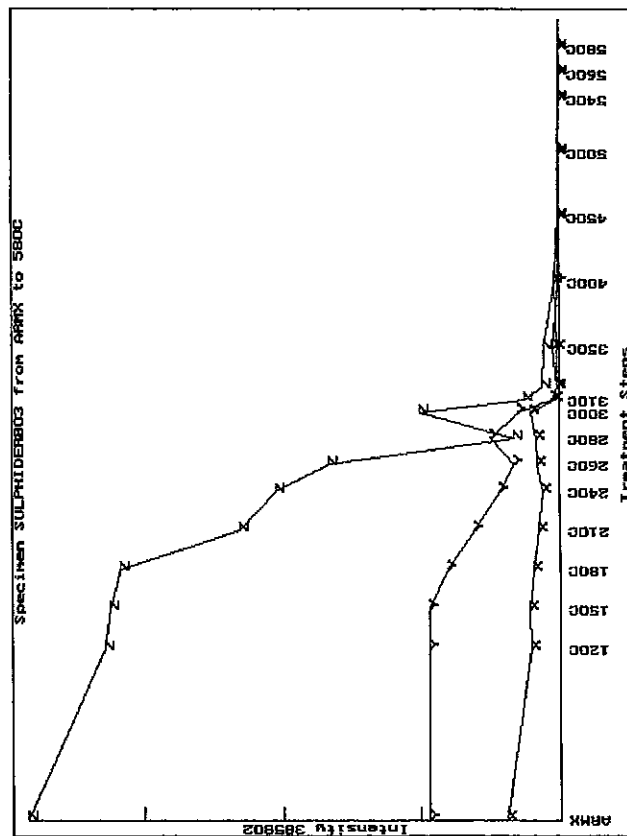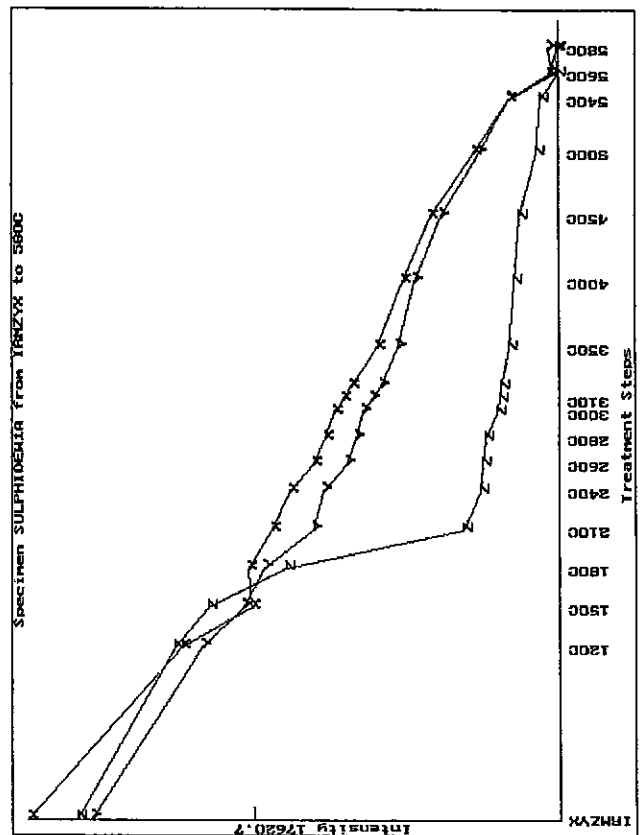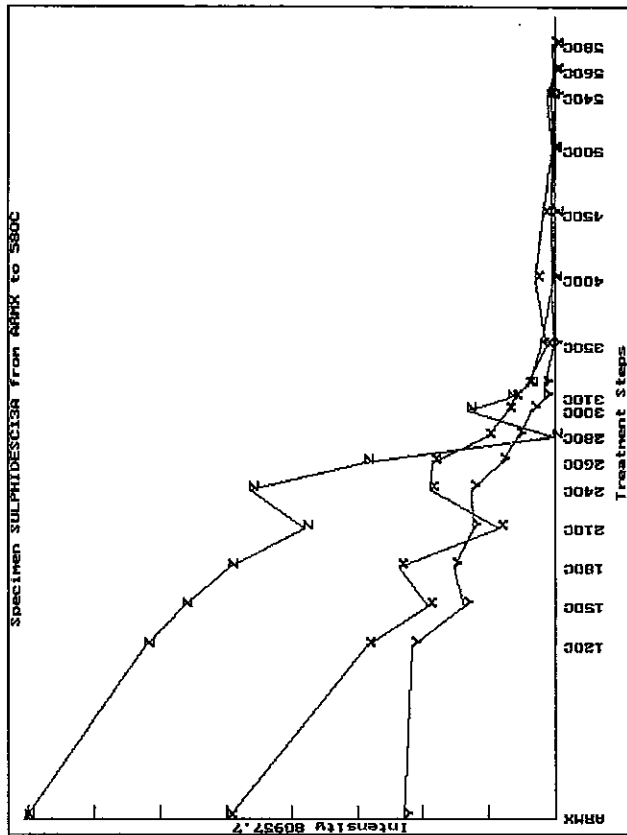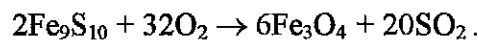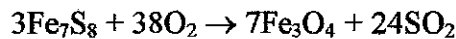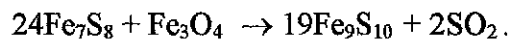
At lower temperatures, below where significant oxidation occurs, peak-type curves due to 5C hexagonal pyrrhotite always show some irreversibility upon cooling from above the apparent Curie temperature. This irreversibility does not reflect chemical changes, but arises from the sluggish kinetics of vacancy diffusion processes that control the antiferromagnetic-ferrimagnetic-antiferromagnetic (5C $\leftrightarrow$ 4C $\leftrightarrow$ 2C) transitions. The characteristic time constants of the diffusion processes are of the order of an hour (Marusak and Mulay, 1980). The degree of irreversibility is accordingly affected by cooling rate - very slowly cooled specimens exhibit almost reversible curves.

Lowrie (1990) analysis involves imparting three orthogonal isothermal remanent magnetisations (IRMs) to a specimen, in successively lower applied fields, followed by thermal demagnetisation. Thermal demagnetisation curves for each of the components (high coercivity, intermediate coercivity and low coercivity) are plotted to identify Curie temperatures and characteristic chemical changes. The combined information on coercivity and unblocking temperatures serves to uniquely identify many magnetic minerals. A particular advantage of the Lowrie method is that new magnetic minerals created by chemical changes during heating do not normally acquire any remanence, because heating takes place in zero field, and therefore do not register in the demagnetisation curves. Thus chemical alteration that may confuse other

thermomagnetic methods does not significantly affect the interpretation. For example, if magnetite is not originally present in the sample, the characteristic rapid unblocking of IRM just below the Curie point of 580°C will not be observed, even if magnetite is produced by alteration during heating. On the other hand, certain characteristic chemical changes, such as the inversion of maghemite to hematite, do register as rapid unblocking of low and intermediate coercivity components between 300°C and 400°C.

Demagnetisation curves for high coercivity (z-axis: > 0.1 T), intermediate coercivity (y-axis: 20 mT - 100 mT) and low coercivity (x-axis: < 20 mT) components are shown in Fig.18. For those specimens with very high IRM intensities, a modification of the Lowrie method was used. Following the standard step of initial saturation of the specimens in a 1 T field along the z-axis, the modified procedure involved imparting anhysteretic remanent magnetisations in a weak DC field, using alternating fields of 100 mT along the y-axis, followed by 20 mT along the x-axis. The effect of using ARMs, rather than IRMs, for the intermediate and low coercivity components is to greatly reduce the overall remanent intensity to levels that can be measured on a cryogenic magnetometer.

Separation of the coercivity ranges for the three components is degraded by strong anisotropy. Because pyrrhotite-bearing ores are generally quite anisotropic, and because orientation of the specimens during remanence acquisition and measurement is critical, the Lowrie plots are somewhat noisy for these small specimens, which were difficult to align very accurately in the magnetometer. For the majority of specimens, the Lowrie plots show almost complete demagnetisation as the Curie point of monoclinic pyrrhotite is approached. The remanent magnetisation is dominated by monoclinic pyrrhotite, except for W1, reflecting the relative effectiveness of monoclinic pyrrhotite over magnetite as a remanence carrier. By contrast, induced magnetisation, in low or high fields, emphasises the contribution of magnetite relative to monoclinic pyrrhotite, because the susceptibility and saturation magnetisation of magnetite are both substantially greater than the corresponding properties of monoclinic pyrrhotite. Residual remanence above 350°C disappears by 580°C, indicating the presence of magnetite in some samples.

In some specimens, the pyrrhotite remanence is predominantly hard, reflecting relatively small grain size, in others it is predominantly soft, indicating coarser grain size for the monoclinic pyrrhotite. Specimen W1A contains traces of magnetite, ranging from single domain (submicron) to multidomain (> 20 μm), but no monoclinic pyrrhotite. It also contains a high coercivity phase that unblocks at ~210°C. This might be due to trace amounts of Cr-magnetite rims on chromian spinel grains, developed during serpentinisation of the host rock.

5. Quantitative Analysis of Monoclinic Pyrrhotite, Hexagonal Pyrrhotite and Magnetite from High Temperature Hysteresis Loops

Table 3 lists the measured saturation magnetisations at room temperature, 150°C, 190°C, 215°C, 240°C, 270°C and 350°C for small subsamples from the collection of pyrrhotite-bearing samples, with the corresponding values for pure phases listed for comparison. Values for the saturation magnetisation of magnetite as a function of temperature were taken from Bleil and Petersen (1982). Corresponding values for monoclinic pyrrhotite were taken from Menyeh and O'Reilly (1995) and for 5C pyrrhotite the measurements of Marusak and Mulay

(1980) were used. The temperatures were chosen to discriminate contributions from magnetite and different pyrrhotite phases most definitively. The contributors to saturation magnetisation (apart from a small, almost constant, paramagnetic contribution) are:

Room temperature:	monoclinic pyrrhotite + magnetite
150°C:	monoclinic pyrrhotite + (Fe-rich hex po; x ≈ 0.06) + magnetite
190°C:	monoclinic pyrrhotite + 5C hexagonal pyrrhotite + (Fe-rich hex po; x ≈ 0.06-0.08) + magnetite
215°C:	monoclinic pyrrhotite + 5C hexagonal pyrrhotite (maximum) + (Fe-rich hex po; x ≈ 0.06-0.09) + magnetite
240°C:	monoclinic pyrrhotite + 5C hexagonal pyrrhotite + magnetite
270°C:	monoclinic pyrrhotite + magnetite
350°C:	magnetite.

Contributions from phases in parentheses are relatively minor compared to 4C and 5C pyrrhotites.

From the thermomagnetic curves, it is clear that significant amounts of Fe-rich (x < 0.1) hexagonal pyrrhotite are not found, except in W1. Thus it is relatively straightforward, using the saturation magnetisations at the above temperatures and the known saturation magnetions of magnetite, monoclinic pyrrhotite and 5C hexagonal pyrrhotite at these temeperatures, to solve for the absolute amounts of each of these phases in each of the measured subsamples.

Some of the samples are very heterogeneous, so the estimated magnetic mineral modes, derived from measurements of hysteresis loops of small (~ 0.1 cm^3) subsamples, are only approximate. The relative proportions of these phases were assumed to be fairly homogeneous, whilst the absolute concentrations are clearly heterogeneous (blebs and veins). That is, wherever pyrrhotite occurs in a sample, it is assumed to occur as a mixture of monoclinic pyrrhotite and hexagonal pyrrhotite in similar relative proportions. The room temperature saturation magnetisation measured for larger (~ 2 cm^3) specimens in a hysteresis loop tracer was used to calculate more representative absolute concentrations of each of the magnetic minerals. Table 4 gives the estimated modal abundances of the magnetic minerals for the subsamples measured in the VFTB and Table 5 lists the estimated modal abundances for the bulk samples, using room temperature saturation magnetisations measured on the larger subsamples in the hysteresis loop tracer, incorporating the relative proportions of the phases from Table 4. It is clear from the results that the hysteresis-based method is much more sensitive to the presence of small amounts of 5C hexagonal pyrrhotite than the thermomagnetic curve method used by Schwarz (1974). When monoclinic pyrrhotite dominates 5C pyrrhotite, the characteristic Λ-peak is not very evident. However, the saturation magnetisation at ~215°C reflects the additional contribution due to the 5C pyrrhotite and can be used to estimate the absolute amount of 5C pyrrhotite. The normalised thermomagnetic curve lies slightly above that associated with pure monoclinic pyrrhotite, but that is not always evident in the curves.

The Mt Isa samples contain very minor amounts of magnetite and varying amounts of pyrrhotite, which appears always to be mixed-phase. Monoclinic pyrrhotite is inferred to be more abundant than hexagonal pyrrhotite in all but one sample, but in those samples with higher pyrrhotite concentrations, hexagonal pyrrhotite is almost as abundant as monoclinic

pyrrhotite. The L2 sample contains minor magnetite, abundant monoclinic pyrrhotite and even more abundant hexagonal pyrrhotite. SC13 contains substantial magnetite and abundant hexagonal pyrrhotite, but very little monoclinic pyrrhotite. W1 contains trace amounts of magnetite as the only ferrimagnetic phase in the temperature range 20-350°C. The abundant pyrrhotite phase in this sample is inferred to be more Fe-rich (i.e. closer to troilite) than the common 5C hexagonal pyrrhotite, which exhibits peak-type thermomagnetic curves. The W1 pyrrhotite could have a composition around $Fe_{11}S_{12}$, or be even more iron-rich.

6. Conclusions

A new method for estimation of monoclinic and hexagonal pyrrhotite contents of sulphide-bearing samples, based on high temperature hysteresis loops has been developed and tested against conventional thermomagnetic methods. The hysteresis method can be shown to be more sensitive and quantitative than other methods and could be routinely applied to determining the magnetic mineralogy of large collections of samples.

The results confirm that mixed monoclinic and hexagonal pyrrhotites are very common in sulphide ores. 5C intermediate pyrrhotite, with composition ~ Fe_9S_{10}, is the most common "hexagonal' pyrrhotite phase in this collection. The Mount Isa copper ores contain mixed pyrrhotites with subequal amounts of monoclinic and 5C hexagonal pyrrhotite, as well as minor amounts of magnetite. Tin ores from Renison also contain mixed pyrrhotites, Scuddles Zn-Cu ore contains magnetite and hexagonal pyrrhotite, without monoclinic pyrrhotite. One magnetic nickel ore from Western Australia contains predominantly 5C hexagonal pyrrhotite, with substantial monoclinic pyrrhotite. The other, weakly magnetic, nickel ore contains traces of magnetite as the only ferrimagnetic phase, with abundant Fe-rich hexagonal pyrrhotite ± troilite.

7. References

Bertaut, E.F., 1953. Contribution à l'étude des structures lacunaires: la pyrrhotine. Acta Cryst., 6, 557-561.

Bleil, U. and Petersen, N., 1982. Magnetic properties of natural minerals *in* G. Angenheister (ed.), Physical Properties of Rocks, Landolt-Börstein Numerical Data and Functional relationships in Science and Technology, Group V: Geophysics and Space Research, Volume 1b, 308-365.

Clark, D.A., 1980. Reliability of susceptibility measurements on conductive samples - a comparison of commercially available instruments. CSIRO Division of Mineral Physics, Restricted Investigation Report 1173R.

Clark, D.A., 1983. Magnetic properties of pyrrhotite - applications to geology and geophysics. M.Sc. Thesis, University of Sydney.

Clark, D.A., 1984. Crystallography and mineralogy of the pyrrhotite group. CSIRO Division of Mineral Physics, Restricted Investigation Report 1557R.

Clark, D.A., 1985. Intrinsic magnetic properties of pyrrhotite. CSIRO Division of Mineral Physics, Restricted Investigation Report 1571R.

Koto, K., Morimoto, N. and Gyobu, A., 1976. The superstructure of the intermediate pyrrhotites. I. Partially disordered distribution of metal vacancy in the 6C type, $Fe_{11}S_{12}$. Acta Cryst., B31, 2759-2764.

Lowrie, W., 1990. Identification of magnetic minerals in a rock by coercivity and unblocking temperature properties. Geophys. Res. Lett., 17, 159-162.

Marusak, L.A. and Mulay, L.N., 1980. Polytypism in the cation-deficient iron sulfide, Fe_9S_{10}, and the magnetokinetics of the diffusion process at temperatures about the antiferro- to ferrimagnetic (λ) phase transition.

Menyeh, A. and O'Reilly, W., 1995. The coercive force of fine particles of monoclinic pyrrhotite (Fe_7S_8) studied at elevated temperature. Phys. Earth Planet. Inter., 189, 51-62.

Power, L.F. and Fine, H.A., 1976. The iron-sulphur system. Part I. The structure and physical properties of the compounds of the low-temperature phase fields. Minerals Sci. Eng., 8, 106-128.

Schwarz, E.J., 1974. Magnetic properties of pyrrhotite and their use in applied geology and geophysics. Geological Survey of Canada, Paper 74-59, 24p.

Schwarz, E.J. and Vaughn, D.J., 1972. Magnetic phase relations of pyrrhotite. J. Geomagn. Geoelectr., 24, 441-458.

Table 1. Densities and Bulk Magnetic Properties for All Specimens

Specimen	Density (g/cc)	Mass k (μemu/g.Oe)	Volume k (μG/Oe)	Volume k (SI)	NRM Intensity (μG)	Q (F = 0.5 Oe)
L2	4.38	2480	10850	0.136		
L2A	4.475	2490	11150	0.140	43270	7.8
L2B	4.664	2280	10650	0.134	41840	7.9
MI01	2.8	168	471	0.0059	60520	257
MI11	2.835	1655	4690	0.0589		
MI11A	3.308	1050	3470	0.0436	15370	8.9
MI11B	3.516	1586	5580	0.0701	50270	18
MI19	2.73	377	1030	0.0129		
MI19A	2.946	94	277	0.0035	21980	159
MI19B	3.023	174	527	0.0066	11070	42
MI20	3.5	3010	10530	0.132		
MI20A	2.883	51	148	0.0019	2740	37
MI20B	2.862	469	1340	0.0169	14550	22
MI55B	4.088	597	2440	0.0306		
MI55B1	3.614	1090	3930	0.0494	6560	3.3
MI55B2	3.882	446	1730	0.0218	4850	5.6
MI56B	3.669	1440	5290	0.0664		
MI56B1	3.492	1350	4700	0.0590	5890	2.5
MI56B2	3.563	1280	4570	0.0574	6336	2.8
MI56C	3.184	950	3030	0.0380		
MI56C1	3.801	968	3680	0.0462	4605	2.5
MI56C2	3.617	1090	3930	0.0493	1690	0.86
RB03	4.202	597	2510	0.0315	2730	2.2
RB03A	3.72	573	2130	0.0268		
RB09	4.303	1070	4610	0.0579		
RB09A	3.431	6960	23870	0.2998	9780	0.82
RB09B	4.403	2580	11340	0.1424	12390	2.2
SC13	3.427	6770	23210	0.2915		
SC13A	4.3	11360	48840	0.6134	201700	8.3
SC13B	4.51	4480	20210	0.2538	215500	21
W1	4.515	26	119	0.0015		
W1A	4.731	34	161	0.0020	57	0.71
W1B	4.735					

Analysis of pyrrhotite - Report Prepared for MIM Exploration

Table 2. Sample Mean Densities, Susceptibilities and Saturation Magnetisations

SAMPLE	Density (g/cc)	Specific susceptibility (µemu/g.Oe)	Volume susceptibility (µG/Oe)	Volume susceptibility (SI)	Js (G)
L2	4.506	2420	10,880	0.137	22.08
MI01	2.800	168	471	0.0059	0.78
MI11	3.220	1430	4580	0.0575	8.08
MI19	2.900	215	612	0.0077	1.18
MI20	3.082	1180	4010	0.0503	8.19
MI55B	3.861	710	2700	0.0339	12.07
MI56B	3.575	1360	4850	0.0609	14.22
MI56C	3.534	1000	3540	0.0445	17.65
RB03	3.961	585	2320	0.0291	6.43
RB09	4.046	3530	13,270	0.167	31.82
SC13	4.079	7540	30,750	0.386	46.08
W1	4.660	30	140	0.0018	0.28

Table 3. Specific Saturation Magnetisations of Pure Minerals and Subsamples as a Function of Temperture

SAMPLE	SPECIFIC SATURATION MAGNETISATION (emu/g or Am^2/kg) *(paramagnetic contribution in 7000 Oe)						
	T = 20°C	T = 150°C	T = 190°C	T = 215°C	T = 240°C	T = 270°C	T = 350°C
Magnetite	92	81.5	79	78	75	72	60
Monoclinic 4C pyrrhotite (Fe_7S_8)	18	13.9	12.1	10.8	9.4	7.4	(0.7)
5C Hexagonal pyrrhotite (Fe_9S_{10})	(0.9)*	(0.9)	2.34	6.7	5	(0.7)	(0.7)
Iron-rich hexagonal pyrrhotite (x < 0.1)	(0.9)	(0.9)	(0.9)	(0.9)	(0.7)	(0.7)	(0.7)
L2	7.34	9.04	6.88	8.12	7.52	4.74	0.14
MI-01	0.155	0.13	0.12	0.11	0.11	0.09	0.004
MI-11A	0.067	0.059	0.059	0.054	0.048	0.043	0.009
MI-19A	0.061	0.051	0.045	0.041	0.043	0.025	0.002
MI-20B	2.25	2.05	1.94	1.89	1.64	1.43	0.021
MI-55B	1.55	1.52	1.45	1.35	1.2	1.02	0.013
MI-56B	4.88	3.95	3.81	3.72	4.74	3.33	0.029
MI-56C	4.9	4.58	4.27	4.02	4.19	3.13	0.037
RB-03	1.72	1.21	1.15	1.19	5.9	1.92	0.13
RB-09A	12.71	11.53	10.89	10.43	11.99	10.89	7.61
SC13B	9.27	8.62	8.62	8.75	9.71	8.93	7.45
W-1B	0.026	0.063	0.058	0.063	0.075	0.077	0.11

Analysis of pyrrhotite - Report Prepared for MIM Exploration

Table 4. Estimated Magnetite, Monoclinic Pyrrhotite and 5C Hexagonal Pyrrhotite Contents of Subsamples

SAMPLE	SPECIFIC SATURATION MAGNETISATION (emu/g or Am²/kg)							INFERRED MAGNETIC MINERALOGY					
	T = 20°C	T = 150°C	T = 190°C	T = 215°C	T = 240°C	T = 270°C	T = 350°C	magnetite (wt %)	mono po (wt %)	Fe_9S_{10} hex po (wt %)	magnetite (vol %)	mono po (vol %)	Fe_9S_{10} hex po (vol %)
L2	7.34	9.04	6.88	8.12	7.52	4.74	0.14	0.23	39.59	54.67	0.20	37.69	52.05
MI-01	0.155	0.13	0.12	0.11	0.11	0.09	0.004	0.01	0.83	0.23	0.00	0.50	0.14
MI-11A	0.067	0.059	0.059	0.054	0.048	0.043	0.009	0.02	0.30	0.15	0.01	0.21	0.11
MI-19A	0.061	0.051	0.045	0.041	0.043	0.025	0.002	0.00	0.32	0.05	0.00	0.21	0.03
MI-20B	2.25	2.05	1.94	1.89	1.64	1.43	0.021	0.04	12.32	7.94	0.02	7.67	4.94
MI-55B	1.55	1.52	1.45	1.35	1.2	1.02	0.013	0.02	8.50	6.19	0.02	7.55	5.51
MI-56B	4.88	3.95	3.81	3.72	4.74	3.33	0.029	0.05	26.86	32.52	0.03	21.43	25.93
MI-56C	4.9	4.58	4.27	4.02	4.19	3.13	0.037	0.06	26.91	24.10	0.04	18.62	16.68
RB-03	1.72	1.21	1.15	1.19	5.9	1.92	0.13	0.22	8.45	73.78	0.18	7.72	67.40
RB-09A	12.71	11.53	10.89	10.43	11.99	10.89	7.45	12.42	7.15	29.93	8.22	5.33	22.33
SC13B	9.27	8.62	8.62	8.75	9.71	8.93	7.45	10.08	0.00	32.13	8.77	0.00	31.50
W-1B*	0.026	0.063	0.058	0.063	0.075	0.077	0.11	0.03	0.00	0.00	0.03	0.00	0.00

*W1 sample consists mostly of iron-rich (x < 0.1) hexagonal pyrrhotite (possibly 6C, $Fe_{11}S_{12}$) ± troilite.

Table 5. Estimated Magnetite, Monoclinic Pyrrhotite and 5C Hexagonal Pyrrhotite Contents of Bulk Samples

SAMPLE	AVERAGE INFERRED MAGNETIC MINERALOGY							
	magnetite (wt %)	monoclinic po (wt %)	5C, Fe_9S_{10} hex po (wt %)	other minerals (wt %)	magnetite (vol %)	monoclinic po (vol %)	5C, Fe_9S_{10} hex po (vol %)	other minerals (vol %)
L2	0.16	26.42	36.49	36.93	0.14	25.89	35.75	38.23
MI01	0.01	1.49	0.42	98.09	0.01	0.90	0.25	98.84
MI11	0.56	11.07	5.80	82.56	0.35	7.75	4.06	87.84
MI19	0.02	2.15	0.36	97.46	0.01	1.36	0.23	98.40
MI20	0.04	14.56	9.38	76.01	0.02	9.75	6.29	83.93
MI55B	0.04	17.14	12.49	70.32	0.03	14.39	10.49	75.09
MI56B	0.04	21.90	26.50	51.56	0.03	17.02	20.59	62.36
MI56C	0.06	27.43	24.56	47.94	0.04	21.07	18.87	60.01
RB03	0.21	7.97	69.62	22.20	0.16	6.86	59.95	33.03
RB09	7.71	4.42	18.52	69.34	6.00	3.89	16.29	73.82
SC13	16.22	0.00	51.54	32.24	12.73	0.00	45.70	41.58
W1	0.06	0.00	0.00	99.94	0.06	0.00	0.00	99.94

Analysis of pyrrhotite - Report Prepared for MIM Exploration